ABSTRACT

Title of Document: FAULT DETECTION AND PROGNOSTICS OF INSULATED GATE BIPOLAR TRANSISTOR (IGBT) USING A K-NEAREST NEIGHBOR CLASSIFICATION ALGORITHM.

Edwin Sutrisno, Master of Science, 2013

Directed By: Professor Michael G. Pecht
Department of Mechanical Engineering

Insulated Gate Bipolar Transistor (IGBT) is a power semiconductor device commonly used in medium to high power applications from household appliances, automotive, and renewable energy. Health assessment of IGBT under field use is of interest due to costly system downtime that may be associated with IGBT failures. Conventional reliability approaches were shown by experimental data to suffer from large uncertainties when predicting IGBT lifetimes, partly due to their inability to adapt to varying loading conditions and part-to-part differences. This study developed a data-driven prognostic method to individually assess IGBT health based on operating data obtained from run-to-failure experiments. IGBT health was classified into healthy and faulty using a K-Nearest Neighbor Centroid Distance classification algorithm. A feature weight optimization method was developed to determine the influence of each feature toward classifying IGBT's health states.

FAULT DETECTION AND PROGNOSTICS OF INSULATED GATE BIPOLAR TRANSISTOR (IGBT) USING A K-NEAREST NEIGHBOR CLASSIFICATION ALGORITHM

By

Edwin Sutrisno

Thesis submitted to the Faculty of the Graduate School of the
University of Maryland, College Park, in partial fulfillment
of the requirements for the degree of
Master of Science
2013

Advisory Committee:
Professor Michael G. Pecht, Chair
Dr. Diganta Das
Professor Patrick McCluskey
Professor Peter Sandborn

Table of Contents

List of Figures

Chapter 1: Introduction

The insulated gate bipolar transistor (IGBT) is a power electronic device introduced in the 1980s [1] that is commonly used in medium to high power applications. IGBT is essentially a switch that turns current 'on' and 'off" and used along with other circuit components to form power supplies, power inverters, and converters. For example, systems that use IGBT devices include motor drives in electric cars, drives of electric locomotives, inverters in welding machines, and inverters of wind turbines.

The semiconductor design of an IGBT consists of an n-channel metal-oxide-semiconductor field effect transistor (MOSFET) serving as the gate which drives the base of a PNP bipolar junction transistor (BJT). An equivalent circuit diagram of the IGBT is shown on Figure 1. A parasitic NPN transistor is integral to the design of the IGBT. Under normal operating conditions, this parasitic transistor is in off position, but under high stress conditions of high temperature and current, the parasitic transistor may turn on and create a latchup failure.

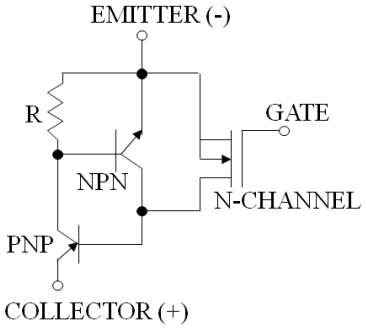

Figure 1 – Equivalent circuit of IGBT showing a N-channel MOSFET at the gate, PNP bipolar transistor, and a parasitic NPN bipolar transistor.

Latchup in IGBTs is due to the activation of the PNPN thyristor structure [2] in the semiconductor. Once activated, large amount of current flows from the collector to

the emitter and the gate no longer has control in stopping the current flow. During a latchup event, current surge overheats the materials in the IGBT packaging causing a destruction of the device by burn-out. The relationship between current and temperature in triggering latchup is explained by Equation 1 [3].

$$I_{CE(Latch)} \propto \frac{V_{bi}}{\alpha_{pnp}\rho_{sp}L_E} \qquad \textbf{Equation 1}$$

where $I_{CE(latch)}$ is the current required to activate the parasitic thyristor, V_{bi} is the built in potential of the N^+-P emitter base junction, α_{pnp} is the gain of the PNP bipolar transistor, ρ_{sp} is the sheet resistance of the p-base and L_E is the length of the emitter. Increase of temperature increases the gain of the bipolar transistor and the sheet resistance of the p-base leading to a reduction in the latching current. Current path during latchup through the IGBT structure is illustrated on Figure 2

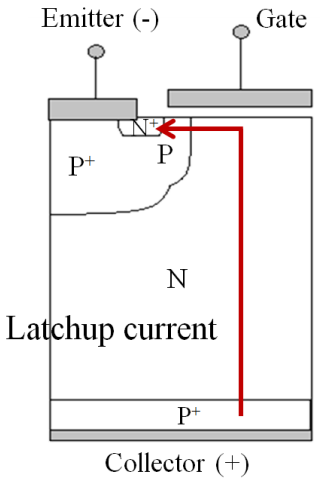

Figure 2 – Illustration of current path during IGBT latchup

Since its introduction the IGBT design improvements have made it more rugged and less susceptible to latchup[2]. However failures continue to occur in the field causing

system downtime. Variations in field loading conditions and part-to-part differences introduce uncertainties in estimating IGBT lifetime. An industry-based survey by Yang et al.[4] in 2001 indicated power transistor as a dominant cause of power converter failures, with IGBT voted as the most popular device. A study by Lu and Sharma[5] in 2009 stated that IGBTs accounted for 38% of inverter failures used in AC motor drives and another study[6,7] employing data from 350 wind turbines found that IGBT converter failures were responsible for 18.9% of the average annual downtime. The ability to assess the degradation of IGBT under its life cycle condition will enable operators to plan for optimal sustainment actions to avoid unexpected IGBT failures.

Motivation and Scope of Study

The conventional approaches in avoiding field failure have pivoted around gathering lifetime data, sometimes from accelerated tests, and making a conservative threshold in deciding a product service life. When data is not available on hand, other common methods in predicting reliability include applying reliability handbooks and physics-based prediction models. By using IGBT failure data obtained from power cycling experiments we show in this study that such approaches suffer from poor accuracy and high uncertainties.

An alternative approach to assessing the reliability of IGBTs is developed using a data-driven method where health state is determined by classifying patterns in data from monitored operating parameters. This approach is different from the conventional reliability approaches in a way that data from individual part is used in conjunction with data from training samples to make a health assessment for that

individual part. The goal of monitoring the individual part is to adjust the prediction model according to the experienced variations in field loading conditions and the part's inherent characteristics. In this study we have developed an alternative approach in avoiding IGBT failures by developing a data-driven prognostic algorithm that monitor IGBT health during operation, warn user of a faulty condition, and provide an estimate of remaining life.

Chapter 2: Power Cycling Experiment

IGBT applications, such as in variable speed motor drives and power inverters, subject the device to fluctuations in power demand and high power density. IGBT loading conditions have caused thermo-mechanical fatigue and high temperature stress as dominant degradation mechanisms [5-9]. This study began with collecting IGBT failure data through a power cycling experiment of 22 new IGBT samples. On and off power cycling creates a non-uniform temperature distribution in the packaging materials and induces thermal stress in material interfaces.

Experimental Setup

The IGBT device used in the experiment was International Rectifier discrete IGBT part #IRGB4045D as shown on Figure 3. It was a discrete field stop IGBT packaged with a parallel freewheeling diode in a TO220 plastic package.

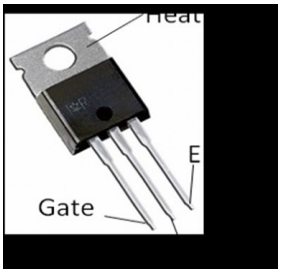

Figure 3 – International Rectifier discrete field stop IGBT used in the experiment. Part# IRGB4045D

Power cycling experiment was conducted between specified minimum and maximum temperatures, T_{Min} and T_{Max}, measured at the device's heat sink. A picture of the thermocouple attachment is shown on Figure 4 where a screw was used to crimp the thermocouple between the device's heat sink and an aluminum heat spreader shown

on Figure 5. Heating process was carried out by switching the IGBT at a specified frequency of 1 kHz or 5 kHz. Once T_{Max} was reached, heating process was stopped and the device was cooled passively using ambient temperature. When the device temperature had cooled down to T_{Min}, the heating process was restarted and the cycle continued up to device failure by latchup or failure to turn on. Figure 6 shows an illustration of the heating and cooling process. Table 1 summarizes the loading conditions performed in the experiment.

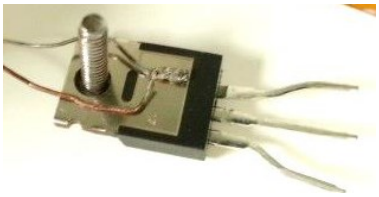

Figure 4 – Placement of thermocouple on the copper heat sink

Figure 5 – Thermocouple fastened to the device's heat sink using a screw and an aluminum heat spreader.

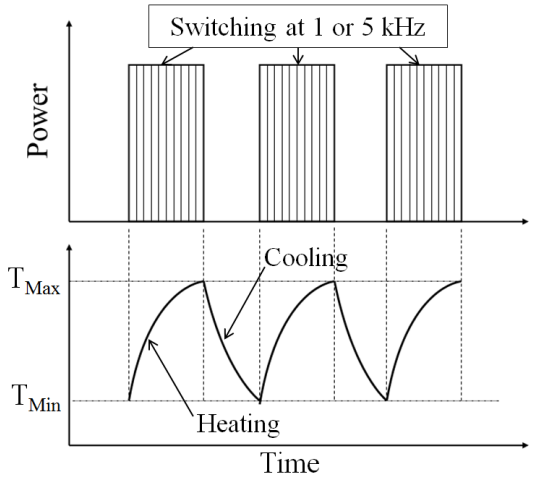

Figure 6 – Illustration of heating and cooling processes in the power cycling experiment

Table 1 – Loading conditions of the power cycling experiment

Temperature Range:	150-200C or 125-225C
Switching Frequency:	1 kHz or 5 kHz
Switching Duty:	50% or 60%
Load:	Resistive and inductive

Parameters monitored during the experiments were the on-state collector to emitter voltage ($V_{CE(On)}$) in volts, on-state collector to emitter current ($I_{CE(On)}$) in amps, off-state collector to emitter voltage ($V_{CE(Off)}$) in volts, off-state collector to emitter current ($I_{CE(Off)}$) in amps, and heat sink temperature (T) in degree Celsius. Figure 7 provides the illustration of the on and off state parameters where V_{GE} plot represents the voltage supplied to the gate to turn on and off the IGBT.

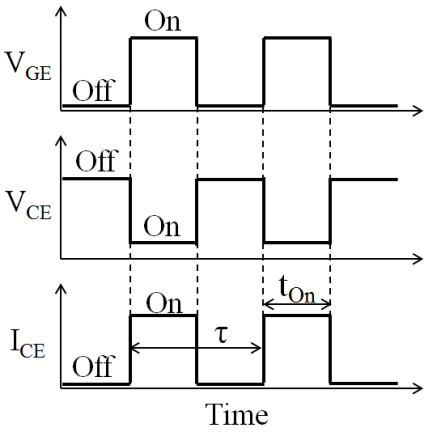

Figure 7 – Diagram of 'on' and 'off' state voltages and currents. A positive bias between the gate and the emitter (V_{GE}) turned the IGBT on.

Experimental Lifetime Results

Lifetime data in number of temperature cycles collected from the experiment are presented on Figure 8 categorized by their temperature profiles to improve visibility for the scale difference in lifetime results. Figure 9 shows the same results presented in number of hours to failure.

a)

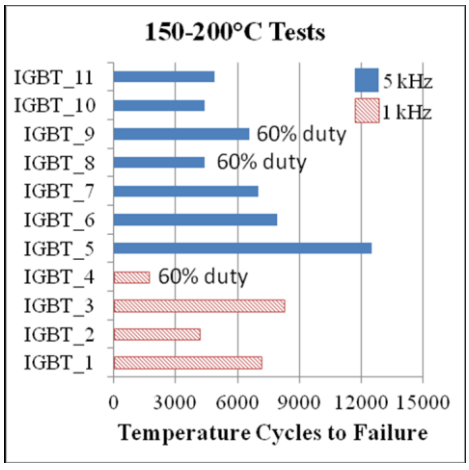

b)

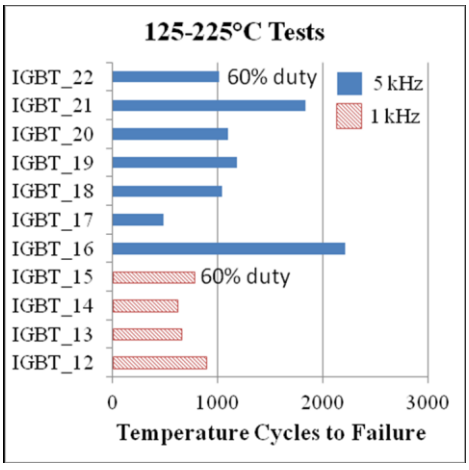

Figure 8 – Experimental lifetime results in number of temperature cycles

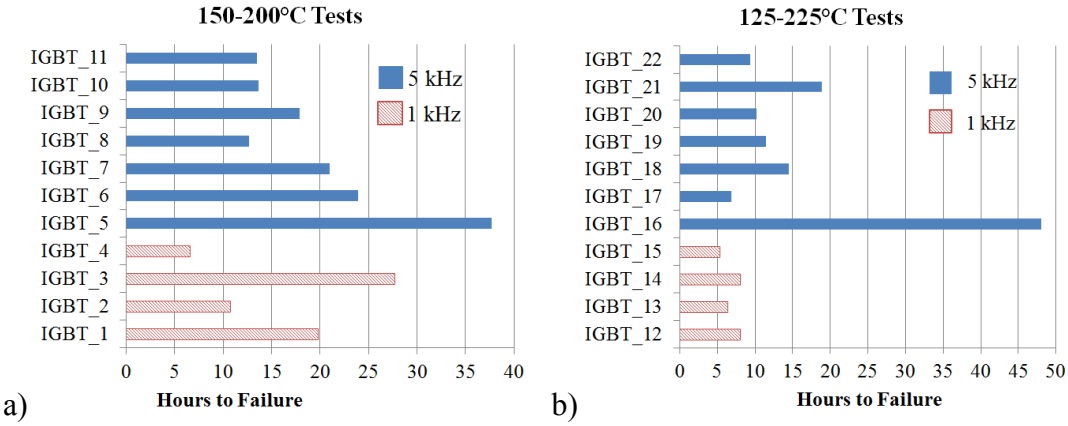

Figure 9 – Experimental lifetime results in number of hours to failure

Chapter 3: Conventional Reliability Prediction Approaches

Conventional Approach 1: Sample Lifetime Statistics

Experimental lifetime data were analyzed statistically by fitting a 2-parameter Weibull distribution using the Reliasoft Weibull++ software as shown on Figure 10. The lifetime data was separated by their temperature loading conditions and the separations in the distribution lines support the hypothesis that they belong in different distributions. The 95% confidence bounds for each distribution were plotted. An overlap in the 95% bounds was present at around the 6% probability line, but for the remaining 94% the separation of the distributions was clear. 2-parameter Weibull distribution was chosen because it fit best to both data sets and agreed with our assumption of wear out failure. 3-parameter Weibull and lognormal distributions also gave a good fit to the data sets however the 3-parameter Weibull fit resulted in a negative gamma shift which suggested failures before the start of experiment and the lognormal distribution did not give an increasing failure rate with time going toward infinity which did not agree with our wear-out assumption.

In the 125-225C data, the mean time to failure (MTTF) estimated by the distribution was 1058 temperature cycles with a 5^{th} to 95^{th} percentile range of 381 to 1815 temperature cycles. In the 150-200C data, the MTTF was estimated to be 6320 temperature cycles with a 5^{th} to 95^{th} percentiles range of 1922 to 11,582 temperature cycles. The MTTF values of the two temperature profiles suggest a reduction in expected lifetime as thermal stress is increased.

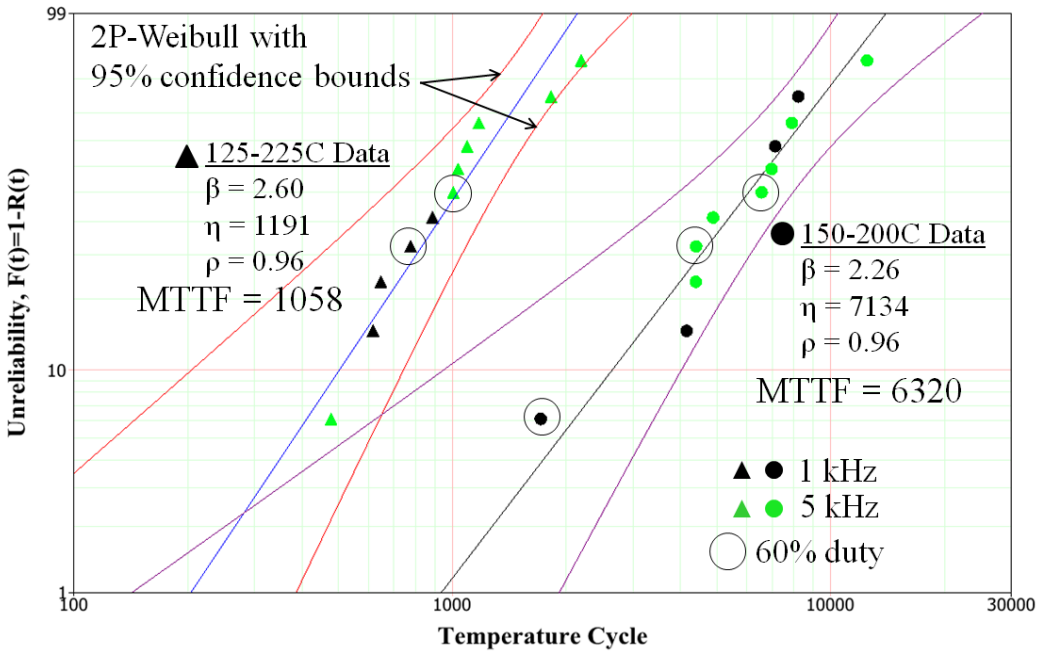

Figure 10 – Statistics of experimental lifetime results using 2-parameter Weibull distributions

A conventional approach in predicting IGBT lifetime based on sample statistics is shown by the experimental results to suffer from wide distributions even under controlled temperature conditions. The width of the 5th to 95th percentile life for the 150-200°C data was 9660 cycles and for the 125-225°C was 1434 cycles. Assigning a product service life using a MTTF value cannot capture the uncertainty introduced by the distribution where IGBTs may fail much earlier or long after the MTTF value. A conservative approach in assigning product lifetime, for example, by using a 5th percentile value of the experimental results would reduce the service life by 2.8 to 3.3 times shorter than the MTTF. Not only would such approach result in wasting useful parts, 5 percent of failure would still occur earlier than the intended service life.

The use of sample lifetime statistics to estimate acceleration factors from exponential or power law lifetime models would be faced with the same challenge of

obtaining results with high uncertainties. An alternative way to predict IGBT failure is to analyze IGBTs individually part-by-part and make a personalized assessment of health based on monitored operating parameters and a data-driven method.

Conventional Approach 2: Physics-of-Failure Based Lifetime Prediction

Thermo-mechanical fatigue due to variations of power dissipation has been identified as a failure mechanism of IGBT [8,9,10,11,12]. One of the components inside the IGBT packaging that degrades due to thermo-mechanical fatigue is the die attach. Degradation in the die attach increases the thermal resistance and electrical resistance between the chip and the IGBT copper base plate which also serves as the collector terminal and the heat sink. Figure 11 shows a schematic cross-section of the IGBT sample in this study and the material compositions as provided by the manufacturer's bill of materials.

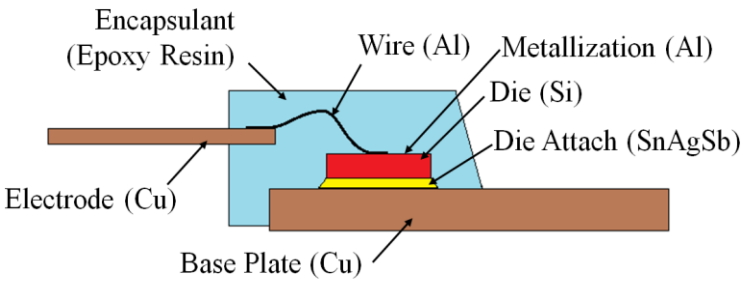

Figure 11 – Schematic cross section of IGBT sample. The copper base plate also served as the collector terminal and heat sink.

Physics based die attach fatigue failure was modeled using the CALCE FAST software. The model was based on the Suhir's [13,14] interface stress equation coupled with the Coffin Manson equation. Model inputs were ΔT, temperature cycling period, material properties and dimensions of the die, die attach, and the

copper base plate. Details of the model input to the software are provided in the Appendix A.

Table 2 shows the lifetime prediction output from the software compared with the MTTFs obtained from the experimental data. As shown from the results, the difference between the physics-of-failure (PoF) predictions and the experimental results were in the order of magnitude. Error of prediction in this method was partly due to latchup failures that were not captured by the die attach PoF model which was developed using failure criteria based on crack size and electrical resistance.

Table 2 – Lifetime prediction results using a die attach fatigue physics-of-failure model compared with MTTFs obtained from experimental data

Temperature	PoF Lifetime Prediction	Experiment MTTF
150-200°C	15,300 cycles	6320 cycles
125-225°C	10,800 cycles	1058 cycles

Degradation in packaging increased the thermal resistance between the chip and the heat sink and consequently increased the junction temperature and device's susceptibility to latchup. This means that even for the same level of die attach degradation, a device that is operated at a higher temperature would have a shorter lifetime compared to a device that is operated at a lower temperature due to its susceptibility to latchup.

In order to relate die attach degradation to latchup failure, junction temperature would need to be modeled as a function of die attach degradation. Although it is not the objective of this thesis to develop this approach, elements that

need to be considered to develop the model are briefly discussed here. Figure 12 shows an equivalent thermal resistance circuit from the junction to the heat sink. Thermo-mechanical fatigue was assumed to produce cracks and delamination in the die attach and over time reduce the effective conducting area of the die attach. When die attach surface reduces, the equivalent thermal resistance of the stack increases and therefore inducing a larger temperature increase from the heat sink to the junction (ΔT_{JS}).

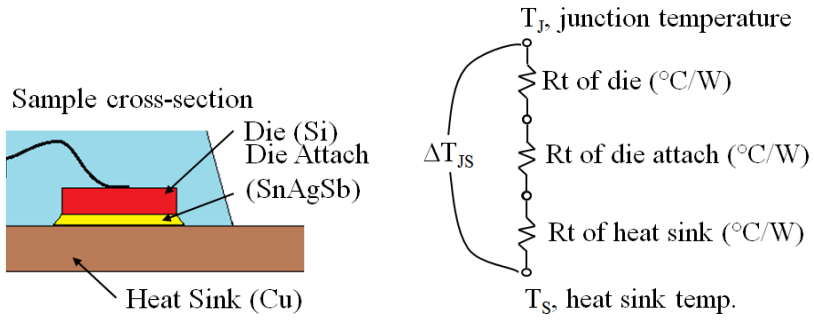

Figure 12 – Layers of materials inside the IGBT packaging and the equivalent thermal resistance circuit.

Figure 13 shows a simulated ΔT_{JS} increase as a function of die attach area reduction due to thermo-mechanical fatigue. Parameters used to generate the simulated plot were based on the materials and power dissipation experienced by the IGBT sample used in the experiment. At a new condition, the thermal resistance from the junction to heat sink was given by the manufacturer's data sheet as 1.94°C/W which produced a ΔT_{JS} of 23.3°C based on a calculated power dissipation of 12.03W. Calculation for the IGBT power dissipation is provided on Appendix B. Upon reduction of die attach area, ΔT_{JS} increased to 59.1°C at 70% area reduction.

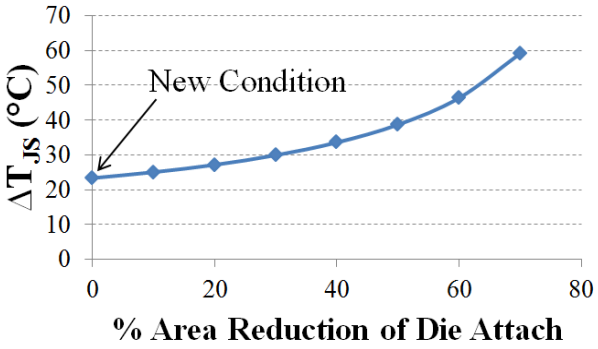

Figure 13 – Simulated increase of temperature difference between the heat sink and junction as die attach area is reduced by degradation

Figure 14 shows an illustration of a latchup occurrence when the highest junction temperature (T_J) in a temperature cycling loading reaches an assumed latchup temperature of 255°C. In this simulation, the heat sink temperature was 200°C. After approximately 8250 temperature cycles, the remaining die attach area had linearly reduced to less than 35% of the original area and the increase of ΔT_{JS} raised the junction temperature to the latchup temperature of 255°C.

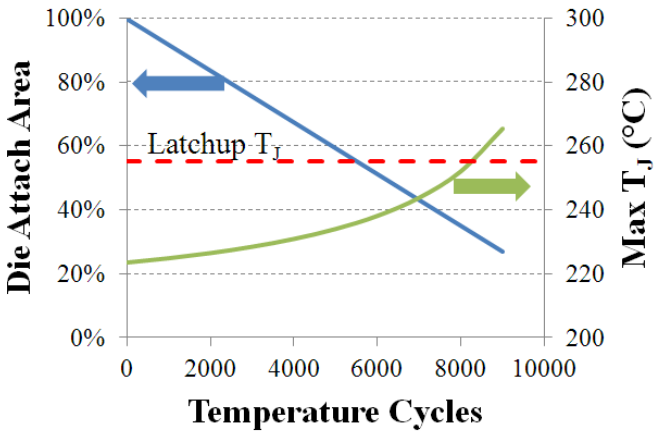

Figure 14 – Illustration of junction temperature reaching a latchup temperature as a result of die attach area reduction.

The outcome of the simulation would vary with changes in power dissipation due to switching frequencies and duty cycle. Results of this simulation are only a

gross approximation of the actual phenomenon and can only be used for illustration purposes. Among the many limitations of this method are the assumptions of linear reduction of die attach area, latchup temperature, constant power loss, constant thermal conductivities, and the equivalent thermal resistance network. To develop an accurate model using this approach would require further investigations into the change of material properties with degradation, the proper thermal resistance network modeling, and other operating aspects. It is not the objective of this thesis to develop such an approach, but the challenges outlined in this section provide the motivation for an alternative approach in predicting IGBT failure by using a data-driven method.

Conventional Approach 3: Military Reliability Handbook

The Military Handbook of Reliability Prediction of Electronic Equipment (MIL-HDBK-217) [15] was published by the Department of Defense to provide a uniform method in predicting the reliability of electronic equipment. Literatures have shown that the MIL217 handbook produces inaccurate results [16,17] and a change notice was released stating that the handbook may only be used for guidance and shall not be cited as a requirement. Nevertheless, the MIL217 still continues to be used by engineers partly due to their ease of use in getting quick prediction results.

The MIL217 provides a set of formulas to estimate the failure rate of electronic equipment including some transistors. In the latest Revision F Notice 2 of the handbook released in 1995, no formula for IGBT is provided therefore, the IGBT was modeled as a series of a MOSFET with a Bipolar Junction Transistor (BJT) to reflect the similar semiconductor configuration of the IGBT. Calculation of failure

rate for discrete semiconductor products is typically expressed using a formula as shown in Equation 2.

$$\lambda_p = \lambda_b \pi_T \pi_A \pi_R \pi_S \pi_C \pi_Q \pi_E \qquad \text{Equation 2}$$

where λ_p is the failure rate of the part, λ_b is the base failure rate for the part and the remaining terms are correction factors for temperature (π_T), application (π_A), power rating (π_R), stress, complexity (π_C), quality (π_Q), and environment (π_E). The failure rate of a MOSFET and a BJT connected in series was calculated by adding the individual failure rates. Since different switching frequencies and duty cycles were employed in the power cycling experiment, the resulting junction temperature was also different for each case due to different power dissipations. Table 3 outlines the output failure rates in units of failures/10^6 hours using the MIL217 formulas for MOSFET, BJT, and the summation of MOSFET and BJT in series under different switching frequencies and duty cycles.

Table 3 – MIL217 failure rate (λ) prediction results (in failures/10^6 hours)

	1kHz, 50%DC	**1kHz, 60%DC**	**5kHz, 50%DC**	**5kHz, 60%DC**
MOSFET	5.68	5.85	5.81	5.98
BJT	1.01	1.04	1.03	1.07
MOSFET-BJT	6.69	6.89	6.84	7.05

Since a constant failure rate is assumed by MIL217, MTTF can be calculated by taking the reciprocal of the failure rate. MTTFs of the MOSFET-BJT model were calculated in Table 4. In comparison with the experimental data, the MTTF from the 150-200°C and 125-225°C data were 18.7 hours and 12.2 hours, respectively, estimated by fitting 2-parameter Weibull distributions on the lifetimes. Very large

differences (4 orders of magnitude) were observed between the MIL217 results and the experimental data. Among the factors that contributed to the inaccuracy of the MIL217 is the lack of temperature cycling as an input loading condition to the provided formulas and where changing the magnitude of ΔT has no effect in changing failure rate.

Table 4 – MIL217 MTTF (1/ λ) results using the MOSFET-BJT model

1kHz, 50%DC	1kHz, 60%DC	5kHz, 50%DC	5kHz, 60%DC
149,543 hours	145,116 hours	146,412 hours	141,924 hours

Summary of the Conventional Reliability Approaches

Three different approaches were discussed in this section based on sample lifetime statistics, physics-of-failure, and a handbook. Sample lifetime statistics obtained from experimental data showed wide distributions of lifetimes even under controlled temperature conditions. Using those statistics to make prediction of lifetime or develop acceleration factor models would result in high uncertainties, unexpected failures, and waste of useful parts. A physics-of-failure approach was demonstrated using a die attach fatigue model and resulted in overoptimistic results partly due to the inability of the model to capture latchup phenomenon. In order to develop a better physics-of-failure approach, further investigations would need to be done to understand the interactions between failure mechanisms, changes in device characteristics with degradation, and equivalent thermal resistance network in the packaging. Investigations on all those issues are beyond the scope of this thesis. A handbook approach was demonstrated using the Military Handbook 217 and results showed a gross overestimation of lifetime partly due to the lack of temperature

cycling as an input loading condition, unavailable model for IGBT, and inaccurate categorizations of the device to fit into the set of criteria written in the handbook.

An alternative approach is needed to predict the lifetime of IGBT considering the part-to-part variations as well as the variations in the loading conditions. In the next section a data-driven approach is proposed to analyze IGBT health individually by considering the operating parameters.

Chapter 4: Review of Data Driven Prognostics Approaches

Prognostics is an approach to assess the reliability of a product in its actual life cycle conditions [18]. A data-driven prognostics utilizes data collected from online monitoring of device operation to determine the health state of the system. Several data-driven approaches reported in literature are summarized here and their limitations are discussed. In the next chapter, a new data-driven method is presented to overcome the challenges faced by the existing methods.

Literature Review for data-driven IGBT Prognostics

Several studies utilized the increase of $V_{CE(On)}$ as a precursor parameter to IGBT failure. Xiong et al. [19] proposed a fault detection method where an increase of $V_{CE(On)}$ by 15% of the initial value is a sign that the IGBT has approached the end of its life. Patil et al. [20]used an increase of $V_{CE(On)}$ by 20% of the initial value as a failure threshold in predicting IGBT lifetime by trending the $V_{CE(On)}$ curve over time with a particle filter regression method. An observation into the power cycling experimental data of this study showed that using a specific percentage threshold of $V_{CE(On)}$ resulted in inconsistent times of fault detection and in some cases missed alarms where the $V_{CE(On)}$ curve never reached the threshold before failure. Figure 15 show several plots $V_{CE(On)}$ values collected at 175°C (mid value of temperature cycling) obtained from the experiments with the +15% and +20% thresholds overlaid. Fault alarms were generated when the $V_{CE(On)}$ curve exceeded the +20% threshold. Two of the plots showed alarms generated at 94% of lifetime and 80% of lifetime. The other two plots showed that no alarms were generated prior to failure. Additional

$V_{CE(on)}$ plots from all experiment samples are provided in a latter section as comparisons with the proposed approach.

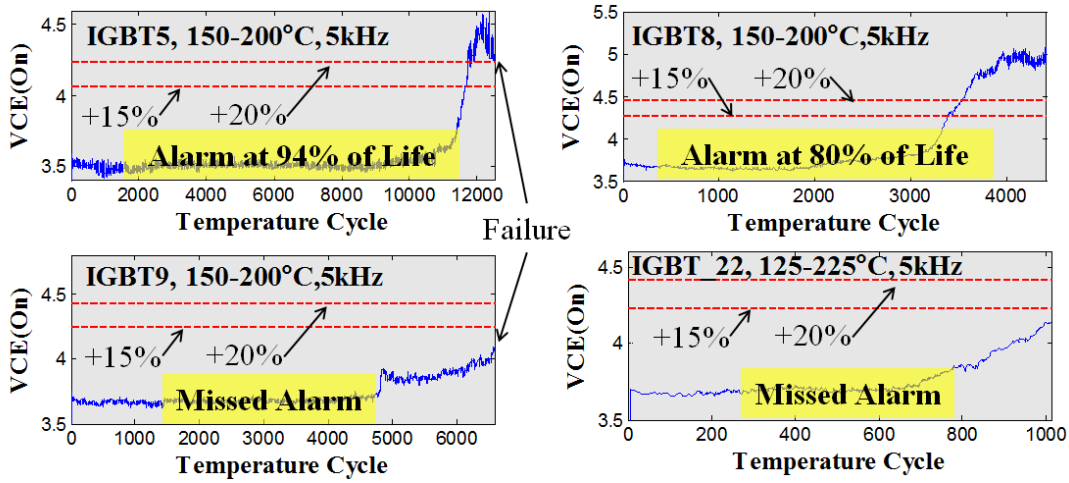

Figure 15 – $V_{CE(On)}$ plots from experimental data of four samples showing different times of detections using the 15% and 20% increase thresholds.

Patil et al in [21] and [22] developed anomaly detection methods for IGBT by calculating the Mahalanobis Distance of $V_{CE(On)}$ and $I_{CE(On)}$ signals collected at a constant temperature. Mahalanobis Distance is a statistical technique to measure the distance of a data point from a set of reference data points normalized by the covariance of the variables. In the works by Patil et al. reference data points were obtained from a healthy condition of the IGBT of the first 50 data points collected in a temperature cycling test. Threshold for anomaly detection in [21] was defined as a deviation in the transformed Mahalanobis Distance above three standard deviations compared to the healthy data. Threshold for anomaly detection in [22] was defined as a deviation in the Mahalanobis Distance value above the 97.5p value of the Chi-Square distribution. A limitation of these methods is the reliance on data collected at a constant temperature while in actual field conditions, IGBT experiences non-constant temperature. Requiring data at a constant temperature would mean

suspending the analysis due to non-ideal temperature, analyzing only data from the reference temperature and ignoring the rest, or having to transform data into the reference temperature by means of interpolation or extrapolation which could introduce error in the process. An adoption of the Mahalanobis Distance methods to the experimental data by including temperature signal resulted in missed and false alarms as shown by Figure 16 and Figure 17.

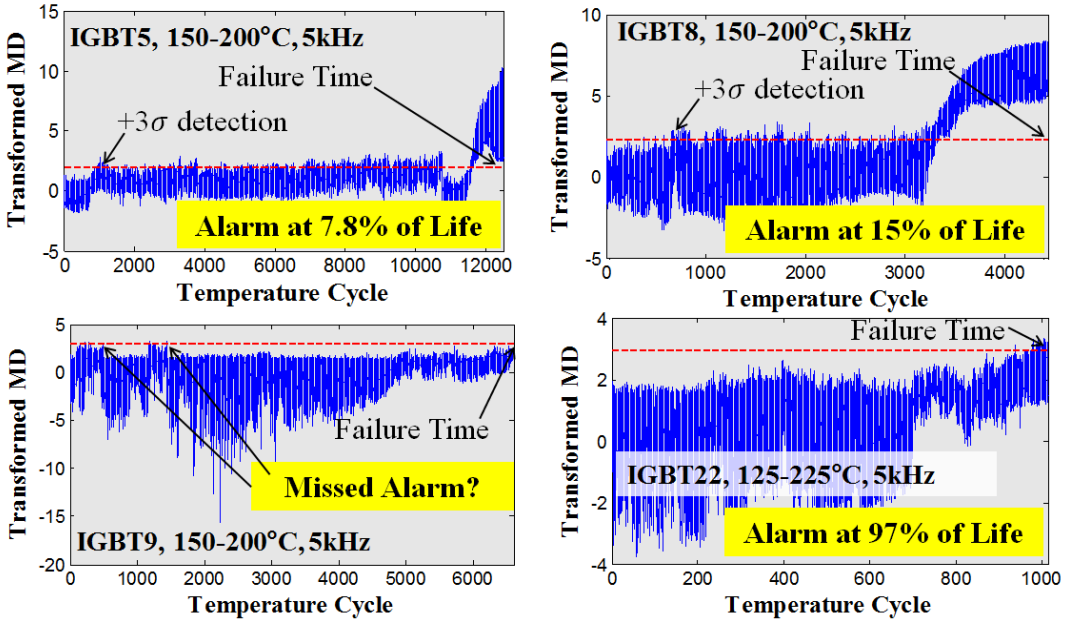

Figure 16 – Applying the transformed Mahalanobis Distance anomaly detection method [21] to experimental data including temperature signal with a 3-standard deviation detection threshold resulted in false, missed, or late alarms.

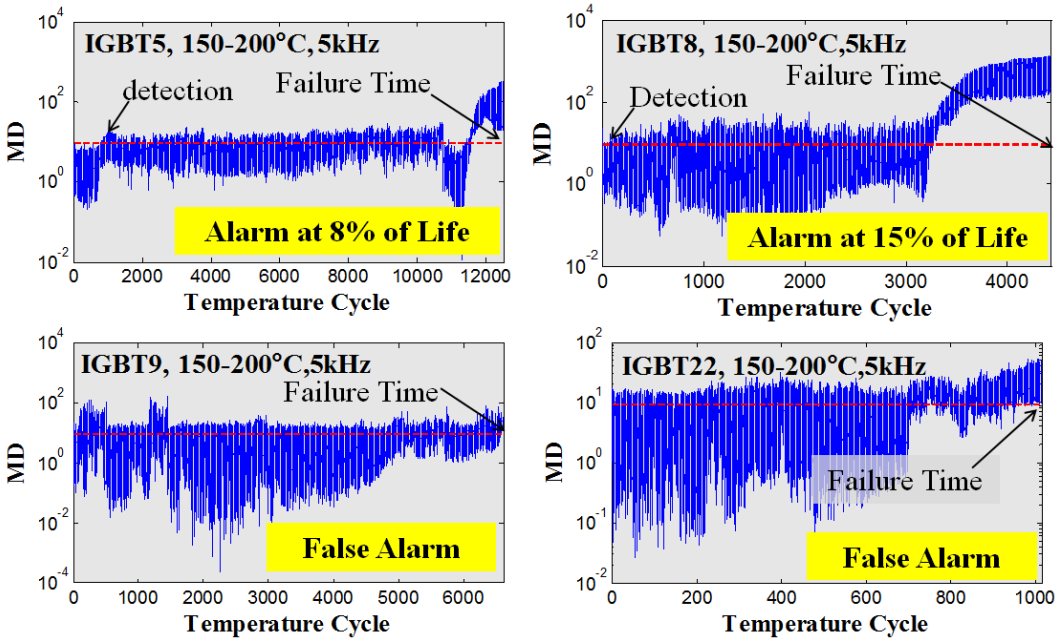

Figure 17 - Applying the Mahalanobis Distance anomaly detection method [22] to experimental data including temperature signal with a 97.5p of Chi-Square distribution detection threshold resulted in false alarms.

Saha et al. [23] developed a method to predict the end of life of IGBT by tracking the decay behavior of the tail current in the off-state. Tracking feature was a curve fit coefficient of the tail current curve. A threshold of failure was developed based on data collected from one IGBT sample as -2.5E5. Figure 18 shows the trend of the feature from the start of the aging experiment until failure. The authors advised that the threshold developed was specific to the given example and not to be applied to other samples due to variations of part-to-part as well as loading conditions.

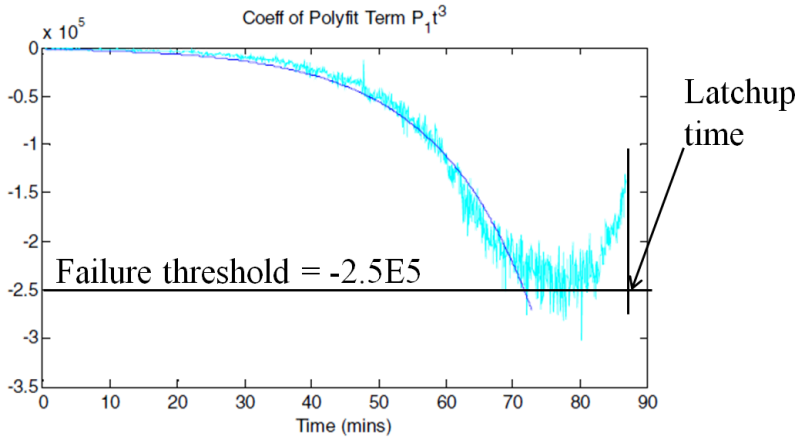

Figure 18 – Predicting IGBT failure by tracking a curve fit coefficient of the off-state tail current to a defined failure threshold [23].

Celaya et al. [24] developed a method to predict the failure of power MOSFETs by defining a failure threshold of when the on-state resistance (ΔRDS_{On}) increases by more than 5% compared to the initial value. Figure 19 shows plots of ΔRDS_{On} obtained from six samples used in [24] where 3 out of the 6 samples failed below the threshold.

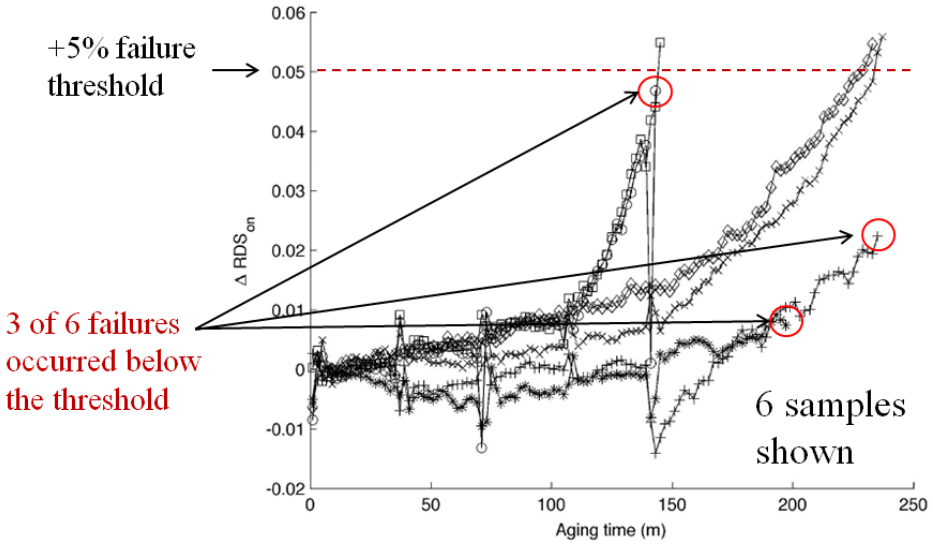

Figure 19 – Failure threshold definition of power MOSFET based on the on-state resistance increase [24].

A similar method was applied to the IGBT experimental data and results were plotted on Figure 20 using detection thresholds of +5% and +50%. Three plots show the on-resistance values collected at 175°C and one plot shows the same data from IGBT 22 plotted using all temperatures. Not only detection times were not consistent, this method was shown to be not robust to varying temperature where deviations due to temperature exceeded the detection threshold.

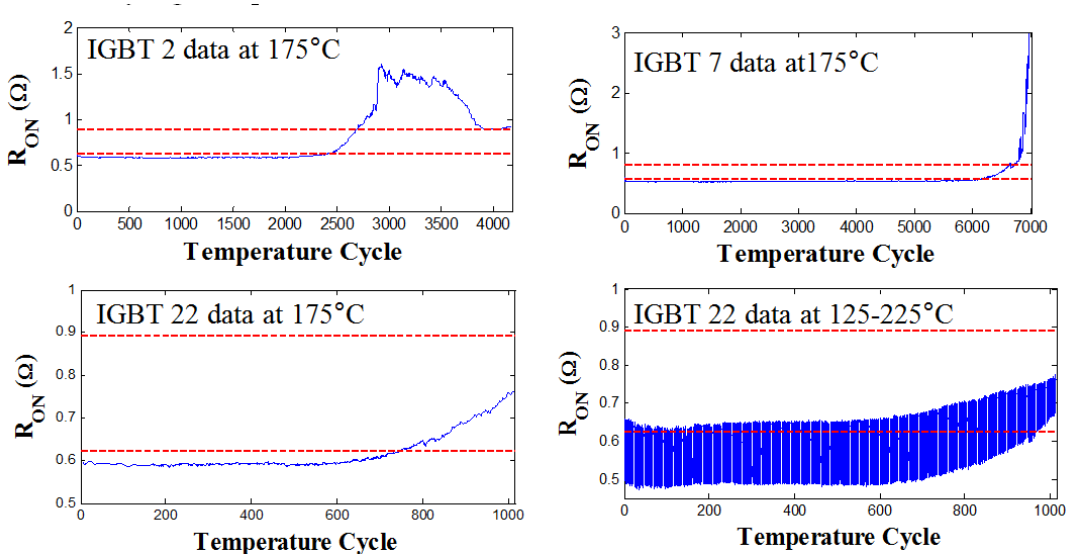

Figure 20 – Applying the increase of on-state resistance failure thresholds of 5% and 50%. Three plots show data collected at constant 175°C temperature and the right bottom plot shows data plotted with varying temperature.

In summary, the common challenge shared by the existing data-driven methods is the determination of threshold for failure detection. Thresholds defined based on a parameter deviation represented only a parametric failure but not the functional failure of the device. When applied to the experimental data, false and missed alarms were generated which in practical applications would lead to wasting good parts as well as unexpected failures.

Chapter 5: Failure Prediction using a K-Nearest Neighbor Centroid Distance Classification Algorithm

In the previous literature review, methods were developed to classify IGBT health based on a parameter deviation. Such approach was shown to produce inaccurate results partly due to variations in the loading conditions of the experimental data which could not be captured only by tracking one operating parameter. To remedy that limitation, a method was developed to map the IGBT health states (healthy and faulty) with multiple operating parameters so that variations of the loading conditions can be accounted for. This mapping process can be regarded as a problem of classification of health states based on input features. A classification algorithm was developed using a K-Nearest Neighbor Centroid Distance approach.

The method developed in this thesis sets itself apart from the previous studies by using functional failure, instead of parametric failure, as the definition for failure. Functional failure here means the IGBT sample could no longer operate due to failure to turn on or failure by latchup. Detection for a faulty condition is not based on a deviation from a healthy reference value as proposed by the existing methods in literature, but rather on remaining life of the device. The training process of the prognostic algorithm proposed in this thesis is divided into steps as shown on Figure 21. Each step is discussed in details in this section.

Figure 21 – Algorithm training steps

Out of the 22 samples used in the power cycling experiment, data from 7 samples were used to train the classification algorithm. The training IGBT sample numbers were 1, 5, 7, 13, 15, 19, and 21. The remaining samples were used as independent data to test the accuracy of the algorithm.

Healthy and faulty classes were defined based on regions of the device life, not on physical damage characteristics of the device. An example of health class definitions is shown on Figure 22 where data from the initial 0-20% lifetime defined the healthy class and 80% lifetime-failure defined the faulty class. Using this health definition scheme means that when operating data from an IGBT is classified into the faulty class, the IGBT is expected to have entered the 80% region of its lifetime and only 20% of life is remaining. This scheme does not discriminate between different failure modes that may be present in the "faulty" region of the training data. In addition to the 0-20% and 80%-failure combination, cases were analyzed using other combinations of healthy and faulty definitions as outlined in Table 5.

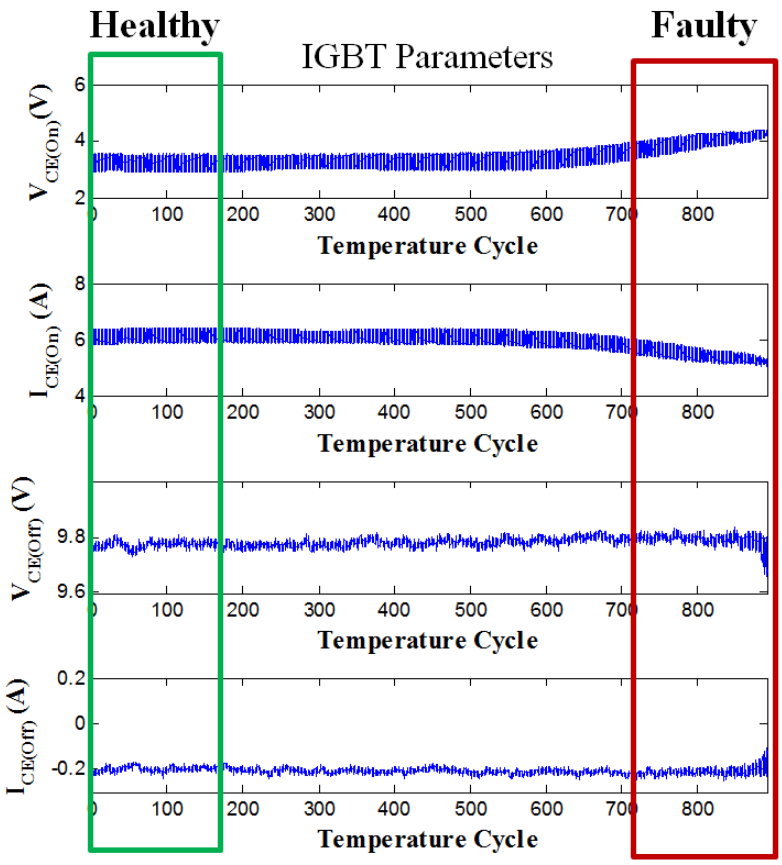

Figure 22 – An example of healthy and faulty class data definitions based on regions of device lifetime. Device failure occurred at the end of the plot at 891temperature cycles.

Table 5 – Different cases of healthy and faulty class definitions

Case	10/90	20/80	30/70	20/90
Healthy Range	0-10%	0-20%	0-30%	0-20%
Faulty Range	90%-failure	80%-failure	70%-failure	90%-failure

Data pre-processing encompassed auto-centering and normalization. Variation in electrical characteristics due to manufacturing can shift initial healthy state (classification) and thus obscure the variations from degradation [24]. To reduce the effects of manufacturing variations, each IGBT electrical parameter was centered by

its initial value recorded at 175°C which is the middle value of the temperature cycle. The middle temperature value was selected as a reference because this was the temperature at which most of the data were expected to operate around. In other temperature loading scenarios, a different value may be selected based on the expected temperature of the operation. After centering, the data of electrical parameters and temperature were normalized to bring them to the same scale by subtracting by the mean and dividing by the standard deviation of the data in the healthy class, as shown by Equation 3.

$$f_i^* = \frac{f_i - \mu_i}{\sigma_i} \qquad \textbf{Equation 3}$$

where f_i^* is the normalized feature, i = 1, 2,..., n parameters, f_i is the original feature vector, μ_i is the healthy mean of f_i , and σ_i is the healthy standard deviation of f_i .

Classification of IGBT health was carried out by a K-Nearest Neighbor centroid distance based classification [25] abbreviated as KNN in this study. KNN is a non-parametric classification technique in machine learning where a new data point is classified based on its proximity to the neighboring data points of known classes. Euclidean distance is calculated from a new data point to the centroid of the nearest neighbors from each class and the new data is classified to the shortest centroid distance as illustrated on Figure 23. In the illustrated classification was performed only on a 2-dimensional feature space but the same concept would extend to a higher dimensional feature as in the case of the IGBT multiple parameter data. A number of nearest neighbors (K) of 3 was used for the illustration, but the actual K would be determined using a sensitivity analysis on the training data.

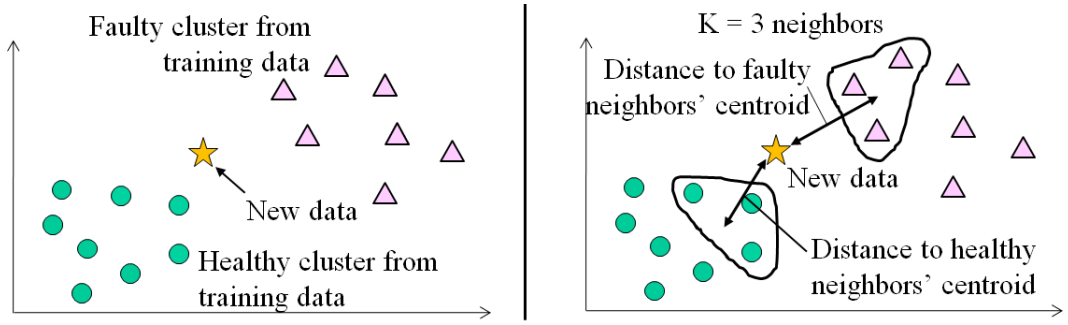

Figure 23 – Illustration of classification using KNN centroid distance in a 2-dimensional feature space with K = 3.

The determination of K depends on the characteristics of the data. A sensitivity study was conducted with a goal to find a value of K at which the classification output is stabilized [26], so that feature weight optimization can be performed afterward. A stable classification output means that the presence of noise would not have a significant impact in changing the location of the nearest neighbors' centroid. Sensitivity analysis was performed by calculating the change in the distance of a test point to the centroid of the nearest neighbors as the value of K was increased by 1 at each step as shown on Figure 24. Stability criterion for K was defined as when at least 90% of the points in the training data, had change in centroid distances of less than 1% of the distance between the healthy and faulty class centroids when all points are included. The Euclidean distance between the healthy and faulty class centroids was found to be 3.95. This is a dimensionless value since the features were normalized. The corresponding 1% stability limits were calculated to be 0.0395.

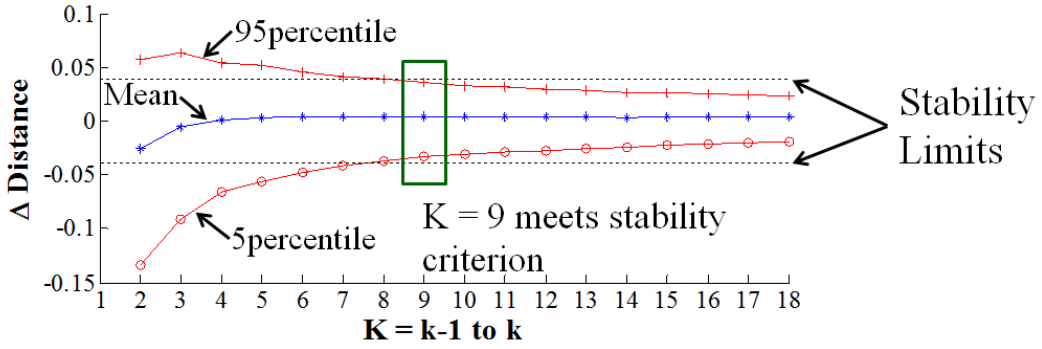

Figure 24 – Selecting K based on sensitivity study for the training data case 20/80

Selection of K is a balancing act between including enough number of neighbors to produce a stable neighbors centroid location and including only neighbors that are "near" to the test point to ensure they are representative of the test point. Figure 25 shows two extreme scenarios of K = 1 and K = all data points in the reference cluster and a balanced scenario of K = 4 where the centroid location is not too sensitive with the presence of noise and at the same time is close enough to the test point. The selection criteria can be summarized as taking the least number of neighbors needed to meet the stability criterion.

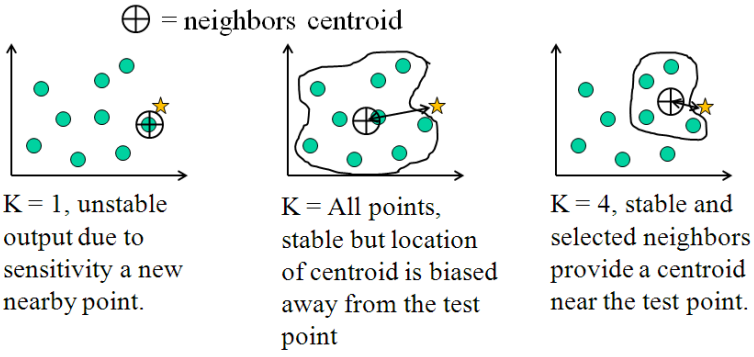

Figure 25 - Considerations in selecting K

Sensitivity study for K was conducted in other training cases (10/90, 30/70, and 20/90). In all cases the selected value of K was 9, except for Case 10/90 where

the selected K was 10. Figure 26 shows the plot of the centroid distance change sensitivity to K for Case 10/90.

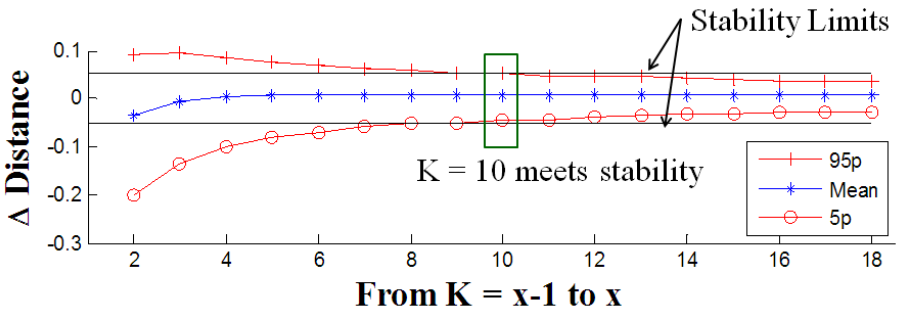

Figure 26 - Selecting K based on sensitivity study for the training data case 10/90

In the proposed data-driven method, IGBT health classes were mapped based on multiple features derived from parameters $V_{CE(On)}$, $I_{CE(On)}$, $V_{CE(Off)}$, $I_{CE(Off)}$, Temperature, and Frequency. Since data-driven methods assume no domain knowledge of the system to understand the level of influence of each feature in determining IGBT health, a statistical approach was developed to assign weights to the features based on their influence in separating the healthy and faulty classes. To that end, an optimization cost function was developed to minimize the classification error given by Equation 4.

$$e(w) = \frac{1}{n}\sum_{i=1}^{n}\frac{D_{i\_True}(w)}{D_{i\_True}(w) + D_{i\_False}(w)} \qquad \textbf{Equation 4}$$

e is mean error, n is total number of training points, i is point index, D_{i_True} is distance of point i to the correct class neighbors' centroid, D_{i_False} is distance of point i to the incorrect class neighbors' centroid, and w is the weight vector. The error is small when the numerator term is small. In other words, when the neighbors' centroid of the correct class is located near the test point, the value of D_{i_True} is small and therefore the overall error term is small. The denominator term normalizes the error in the

numerator by the total distance of the correct and incorrect class neighbors. Different values of feature weights were varied between 0 and 1 to obtain the minimum value of mean error.

An illustration to explain the basic working principle of the feature weight optimization is presented on Figure 27. In the illustration two classes of data are given as class A and class B. These classes consist of data composed of two variables (or features) x and y plotted on the 2-dimensional feature space. In this simplified case, a visual observation shows that separation between classes A and B is predominantly determined by variations in the y axis. Moving right or left on the x axis does not differentiate class A from B. This means variable y has an influence in classifying data while variable x only introduces noise. In some cases, including Δx in distance calculation can result in misclassifying a Class B test point as Class A due to the extra distance introduced by Δx. The optimization algorithm would identify the influence of each feature and automatically assign a small weight to variable x, in this case zero. As a result, any variation in the x direction is removed from further analysis and classification decision is only based on variations in the y direction.

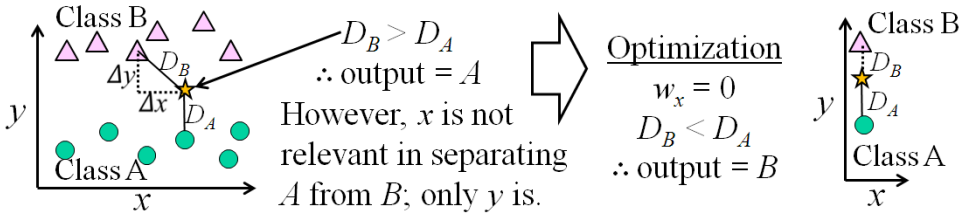

Figure 27 - Two-dimensional illustration of the feature weight optimization process

The basic working principle of the feature weight optimization was applied to the IGBT features in a six-dimensional feature space since there were six features developed from the operating parameters. The resulting optimized weights for each

training data case are presented on Table 6. From the optimization output, $V_{CE(Off)}$ and $I_{CE(Off)}$ were found not to be relevant in determining IGBT health and therefore were removed from analysis by giving them zero weights.

Table 6 - Optimized feature weights for the corresponding IGBT operating parameters (columns) for different training cases (rows)

Training Data	$V_{CE(On)}$	$I_{CE(On)}$	$V_{CE(Off)}$	$I_{CE(Off)}$	Temp.	Freq.
10/90	0.760	0.980	0	0	0.970	1.000
20/70	0.600	0.975	0	0	0.930	0.915
20/80	0.755	0.940	0	0	0.970	1.000
20/90	0.480	0.970	0	0	0.965	1.000
30/70	0.835	0.995	0	0	0.945	0.990

Output of the KNN classification were in a binary format of 0 for healthy and 1 for faulty. The binary output was converted into a continuous Fault Level by taking a moving average of the binary output over time with a window of 100 data points (approximately 5 temperature cycles). The purpose of converting the binary output into a continuous Fault Level is to enable the use of detection thresholds that would otherwise be rife with false alarms if the classification output was fluctuating zeroes and ones. Figure 28 shows an example plot of Fault Level versus temperature cycle. An anomaly was declared when Fault Level > 0.5, i.e. when more than 50% of data points in the moving window belonged to the faulty class. A fault was declared when Fault Level > 0.9, i.e. more than 90% of data points in the moving window belonged to the faulty class.

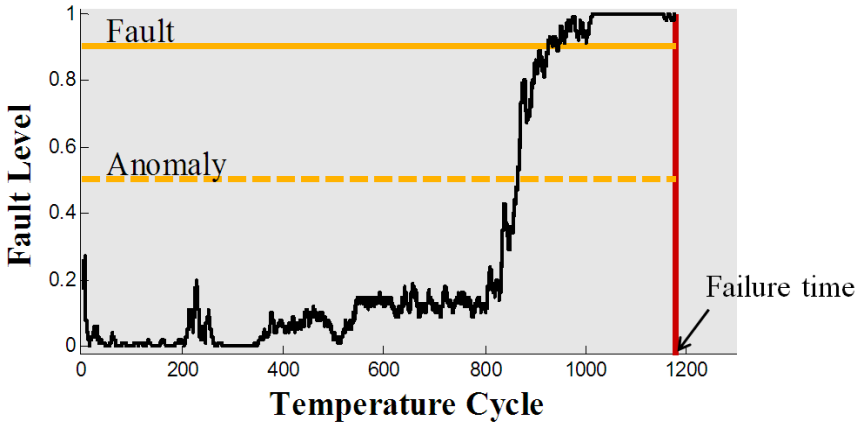

Figure 28 - Example of classification output plot where anomaly and fault detections are defined using the 0.5 and 0.9 thresholds.

The classification scheme was applied to the training data and times at fault detection were recorded in units of percentage of life. The remaining useful life (RUL) was calculated as the time span between the fault detection and device failure. RUL values were normalized by individual lifetimes in units of percentage life. The RUL calculation can be summarized by the expression: RUL = 100% - % Life at Fault Detection. Table 7 gives the RUL values upon fault detections for the seven training IGBT samples using training case 20/80. A normal probability distribution was fitted to the RUL values where mean and standard deviation were calculated. Histogram and the fitted normal probability density function (pdf) are shown on Figure 29.

Table 7 - RULs of training samples for training data case 20/80

Training IGBT #	RUL (%Life)
IGBT 7	12.1%
IGBT 19	17.2%
IGBT 21	17.9%
IGBT 15	24.2%

IGBT 1	24.9%
IGBT 5	26.0%
IGBT 13	31.2%
μ =	**22%**
σ =	**7%**

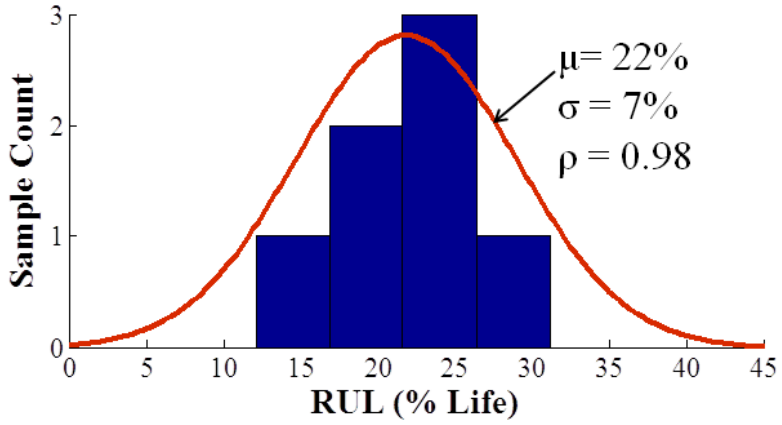

Figure 29 - RUL histogram and fitted normal pdf for the training data case 20/80

The distribution of normalized RULs obtained from the training samples was assumed to represent the distribution of RULs of the population of IGBT parts used in the experiment upon fault detections. It was expected that the standard deviation of RULs obtained from new data would be higher than the training because the algorithm was trained to best fit the training data. In the next section results from applying the developed algorithm to new data are presented.

Chapter 6: Prediction Results of New Data

Of the 22 IGBT samples tested in the power cycling experiment, 7 were used to develop and train the algorithm and the remaining 15 were treated as a new data set to test the accuracy of the developed algorithm. Applying the same classification scheme developed in Chapter 5 and using training case 20/80, the algorithm was able to detect faults prior to failure in 13 of the 15 test samples as outlined on Table 8. Two missed alarms occurred from IGBT# 10 and 20. The actual RUL value for each sample is shown in the table calculated by the time span between fault detection and failure. Any difference between the actual RUL and the mean RUL of 22% from the calculated training data was the error in the prediction, since any new sample that was detected for fault was assumed to have 22% remaining life.

Table 8 - Fault detection of new data and the actual RULs based on training case 20/80

IGBT #	Actual RUL (%Life)
14	2.4%
6	8.6%
17	11.4%
3	17.3%
22	23.3%
11	25.4%
12	25.7%
9	26.8%
8	33.9%
16	36.1%
4	37.6%
2	40.1%
18	43.9%
10	Missed
20	Missed

In order to obtain a statistical evaluation of the prediction error, the distribution of the actual RULs upon fault detection was compared to the training RUL distribution. Figure 30 shows the normal cumulative density functions (CDFs) for the training and new data RULs. Any misalignment in the two curves represents the error of the prediction. At the 50% probability line lie the mean values of the two distributions. Shift between the mean values defines mean error of the prediction.

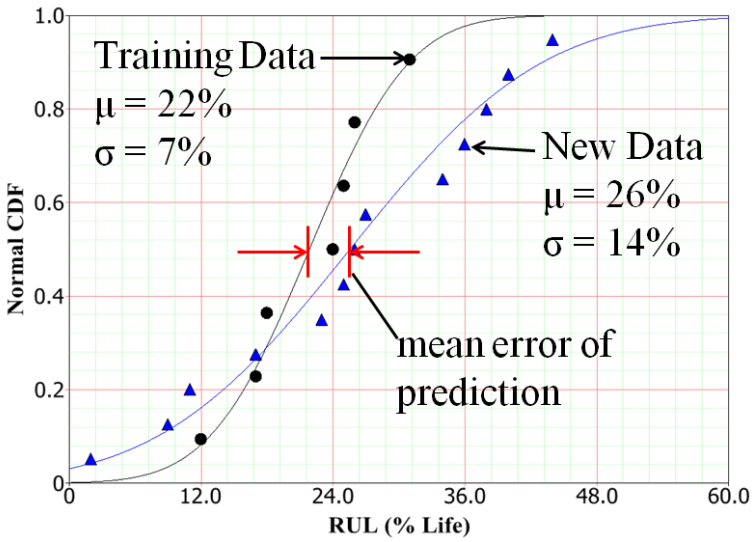

Figure 30 - RUL prediction error evaluation by comparing the CDFs of the training RUL and new data RUL (20/80 training case)

An alternative way to present the prediction results is by plotting the probability density functions (pdf) of the two distributions. Figure 31 shows the histogram of the new data RULs overlaid with the fitted pdf's. As expected the new data distribution featured a wider distribution quantified by the larger standard deviation. The mean RUL prediction error was 4% life. This error is separate from the missed alarm errors from IGBT# 10 and 20 where the algorithm failed to generate

any RUL prediction. Statistical error evaluations for other training cases are presented on Figure 32 to Figure 34.

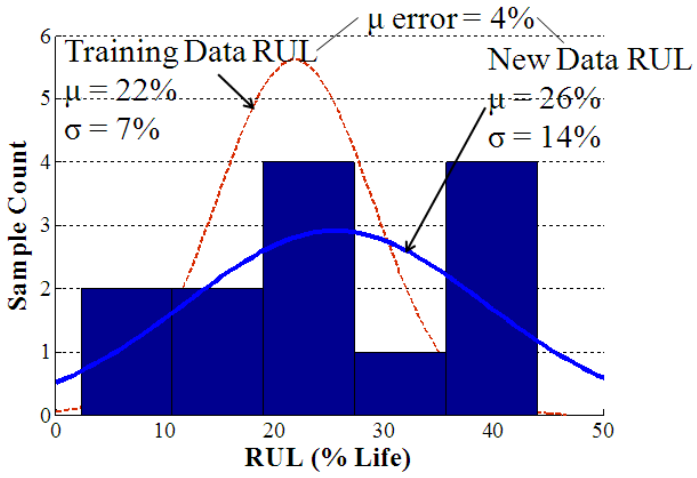

Figure 31 - Prediction error evaluation showing histogram of new data RULs fitted with normal pdf compared to the training data pdf (20/80 training case).

IGBT #	Actual RUL (%Life)
14	7.70%
6	9.45%
17	11.62%
3	24.16%
22	26.91%
11	28.40%
12	36.64%
9	36.84%
8	38.91%
16	39.25%
4	41.61%
2	43.86%
18	44.33%
10	Missed
20	Missed

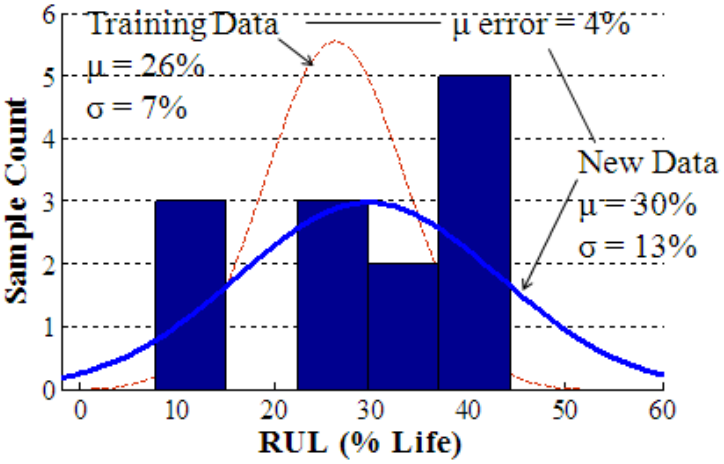

Figure 32 Prediction error evaluation showing histogram of new data RULs fitted with normal pdf compared to the training data pdf (30/70 training case).

IGBT #	Actual RUL (%Life)
17	6.6%
6	7.8%
12	15.5%
3	15.6%
22	18.6%
11	24.0%
9	26.7%
8	28.7%
16	33.9%
4	34.0%
18	34.9%
2	38.9%
10	Missed
14	Missed
20	Missed

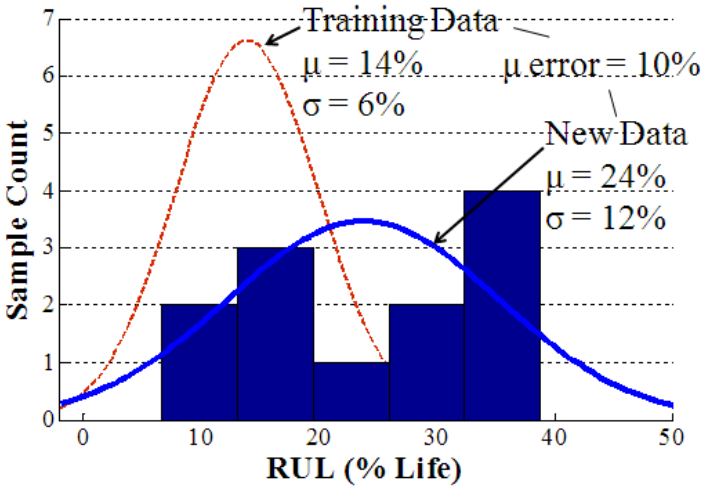

Figure 33 - Prediction error evaluation showing histogram of new data RULs fitted with normal pdf compared to the training data pdf (20/90 training case).

IGBT #	Actual RUL (%Life)
6	7.9%
17	11.6%
3	16.0%
12	16.3%
22	20.9%
11	24.2%
9	26.7%
8	30.0%
4	34.1%
16	34.1%
18	36.8%
2	38.9%
10	Missed
14	Missed
20	Missed

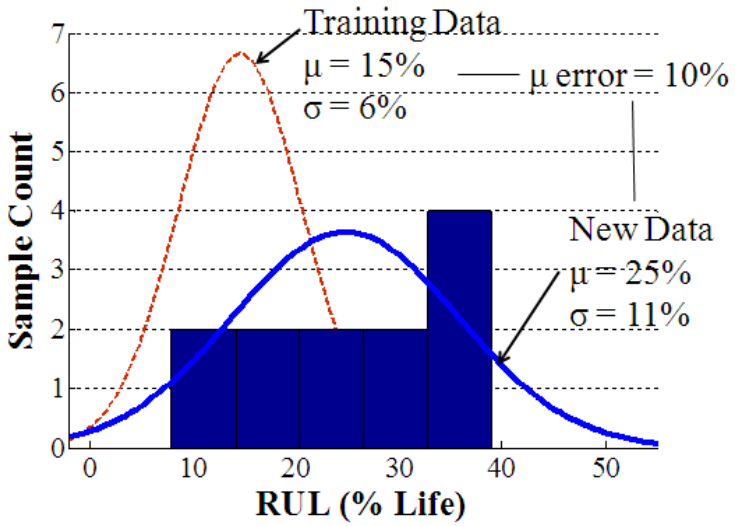

Figure 34 - Prediction error evaluation showing histogram of new data RULs fitted with normal pdf compared to the training data pdf (10/90 training case).

The resulting means and standard deviations from Figure 31 to Figure 34 are summarized on Table 9. The number of missed alarms was increased from 2 to 3 in cases where faulty class was defined using 90% life – failure in comparison with other faulty class definitions. The higher number of missed alarms was due to the less sensitive fault detection where degradation had to reach an advanced state (90% lifetime) before the IGBT could be classified as faulty. From comparison of mean errors, cases 20/80 and 30/70 had the lowest error of 4% underestimation of RUL. In both cases the number of missed alarms was two. The resulting RUL of new data for case 30/70 showed an advantage over the 20/80 case in terms of longer lead warning time prior to failure at 30% mean RUL and a lower variation in predicted RUL with a 13% life standard deviation.

Table 9 – Comparison of training and new data RUL distributions for different training cases

	Training Data		**New Data**		
Case	μ RUL	σ	μ RUL	σ	# Missed Alarms
10/90	15%	6%	25%	11%	3
20/80	22%	7%	26%	14%	2
20/90	14%	6%	24%	12%	3
30/70	26%	7%	30%	13%	2

An example of a successful failure prediction is shown on Figure 35 for IGBT# 22 where fault was detected 778 cycles, mean failure time was predicted at 997 cycles, and the actual failure occurred at 1014 cycles. The error of the failure time prediction was 17 cycles. Not only the algorithm was able to give an early warning for failure, it also provided an estimate of remaining useful life which could be valuable information for operators in planning for sustainment actions. The same

figure also shows the corresponding $V_{CE(On)}$ and $I_{CE(On)}$ parameters of the IGBT. Several methods identified in the literature review employed a percentage increase in $V_{CE(On)}$ as a criterion for faulty IGBT. A +20% $V_{CE(On)}$ threshold was calculated to be 4.5 V. The plot shows that $V_{CE(On)}$ never reached 4.5 V even until failure. Using a +20% threshold method would have led to a missed alarm for this sample.

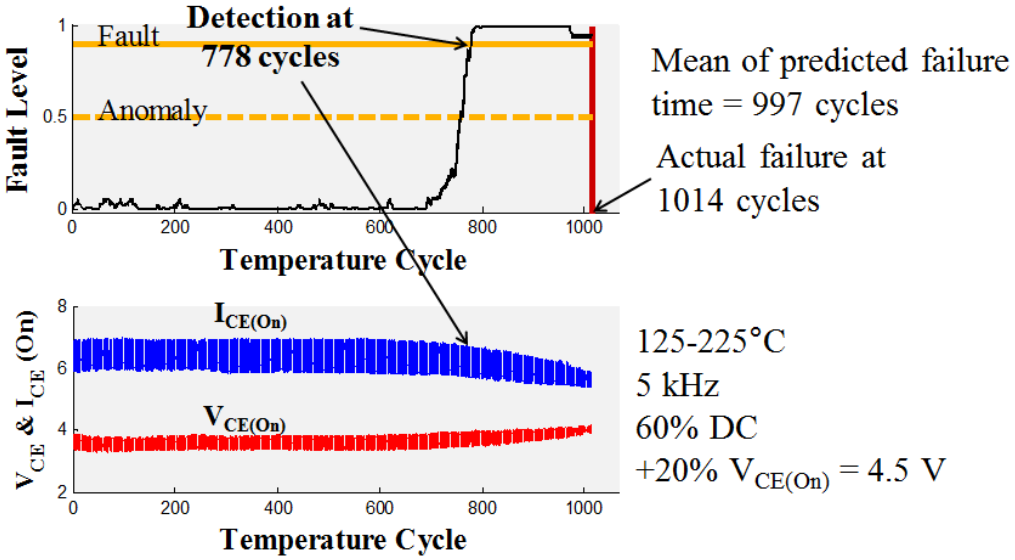

Figure 35 – Successful fault detection and failure prediction for IGBT# 22 using the KNN classification algorithm. An existing method based on +20% increase in $V_{CE(On)}$ threshold is shown to fail to generate detection before failure (training case 20/80).

An example of a poor failure prediction is shown on Figure 36 for IGBT# 14. In this sample, the algorithm successfully detected fault prior to failure but the estimated RUL of 171 cycles was too long compared to the actual RUL of 15 cycles. A look into the $V_{CE(On)}$ and $I_{CE(On)}$ showed small drifts over time until failure. The KNN algorithm had an advantage over the +20% $V_{CE(On)}$ detection method by being able to detect a fault prior to failure.

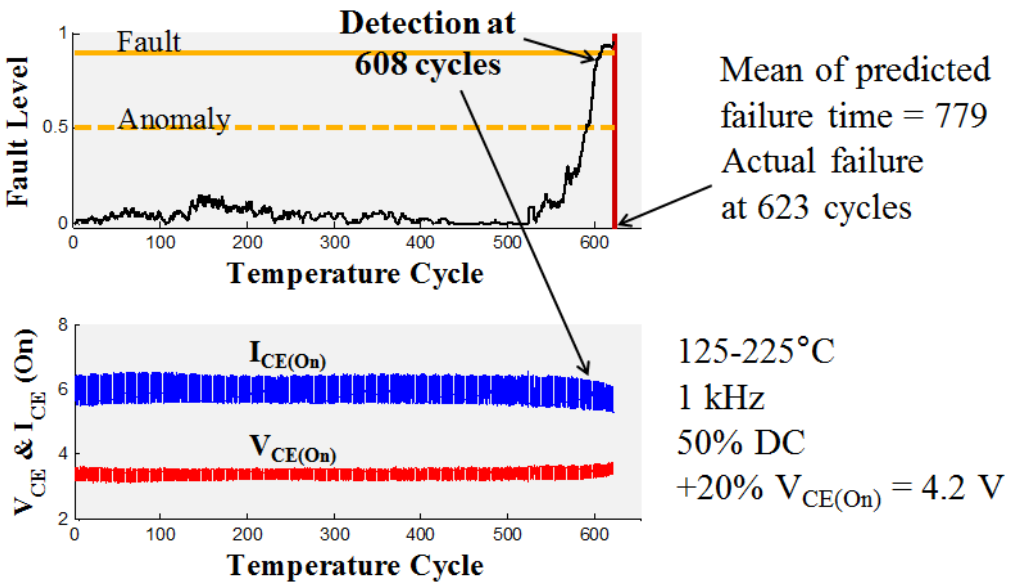

Figure 36 – Successful fault detection before failure for IGBT#14 but a poor prediction of failure time. Mean predicted failure time was 779 cycles and actual failure occurred at 623 cycles (training case 20/80).

Additional fault detection and failure prediction output plots for the 20/80 training case are provided in Appendix C. The KNN algorithm was able to detect faults prior to failure in all samples (except IGBT# 10 and 20) including those where the +20% $V_{CE(On)}$ method failed to detect. In IGBT# 10 and 20 both the KNN and the +20% $V_{CE(On)}$ method produced missed alarms.

Summary

In this study a data-driven health classification approach was developed to detect imminent failures in IGBTs and provide an estimate of remaining useful life. Healthy and faulty classes were based on the percentage of lifetime of the device. When an IGBT was classified as faulty, its remaining life was assumed to follow the distribution calculated from the training data. Classification was performed using a K

Nearest Neighbor centroid distance based algorithm. Features relevant to classifying IGBT health were identified statistically using a feature weight optimization algorithm. Switching frequency was found to be a relevant feature for health classification and this finding was never reported before in literature. The role of switching frequency in determining IGBT health state was hypothesized due to its effect on changing device power dissipation and the time length the chip was exposed to the on-state short circuit.

The developed optimization and classification algorithms successfully detected faults prior to failure in 13 out of 15 new test samples using the 20/80 or 30/70 training data cases. In the sample were faults were successfully detected, mean error in the failure time prediction was 4% life for both 20/80 and 30/70 training cases. The 30/70 training case provided a mean lead warning time 30% remaining life at the time of fault detection.

Chapter 6: Contributions and Future Work

The main contribution of this work is the development and implementation of a prognostic method to IGBT data with varying temperature and loading conditions such as switching frequency, duty cycle, and applied voltage where existing methods were shown to suffer from missed and false alarms. The ability to analyze IGBT health at varying conditions enables a field-ready solution to prognostics and health management. Predicting the time of IGBT functional failure, as opposed to parametric failure criteria employed in existing methods, provided an objective assessment of the end of life of the IGBT independent of user's design criteria.

A second contribution of this work is the development of an optimization based method to determine feature weights for distance-based classification. Not only feature weights can identify the influence of each feature to health classification, it can also be used as a feature selection process where features with weights below a certain low threshold are discarded, thereby reducing costs involved in acquisitioning and processing data and improving classifier's efficiency. The feature weighting algorithm also allows an assessment of new features toward improving health classification as they become available in the future.

Future Work

Further investigation is needed to find the root cause of the missed alarm cases and develop new features or algorithm that can take into account of these special cases. In order to better replicate realistic field loading conditions, additional test scenarios would need to be performed including changing the IGBT switching

duty cycle based on a specified power output demand; and heating and cooling the IGBT sample by increasing and lowering the power demand rather than turning it on and off. Such variations in loading conditions can introduce new degradation patterns on the IGBT may require the algorithm to adapt to new scenarios.

In this work, each IGBT sample was analyzed individually by monitoring the individual parameters. In many field applications, several of IGBTs are connected in different circuit configurations to achieve different functions. Monitoring individual parameters introduces a new challenge to circuit designers that needs to be further investigated.

Appendices

Appendix A: Input attributes to CALCE FAST die attach fatigue model

Die Attributes (Silicon, Si)

Die thickness = 62 μm = 62E-06 m (from lab measurement)

Elastic modulus = 112.4 GPa = 112.4E+09 Pa (from Matweb)

Poisson's ratio = 0.280 (from Matweb)

CTE = 3.61 μm/m-°C = 3.61E-06 (at 227°C from Matweb)

Die length = 2358 μm = 2.358E-03 (from lab measurement)

Die width = 1980 μm = 1.98E-03 (from lab measurement)

Die Attach Attributes (Sn65Ag25Sb10)

Tensile fatigue strength = 117.2 MPa = 117.2E+6 Pa (from Indium Corp. Indalloy 209 solder)

Die attach thickness = 50 μm = 50E-06 m (from lab measurement)

Elastic modulus = 18200 MPa = 18.2E+09 Pa (from CALCE FAST library for SnAg solder)

Poisson's ratio = 0.34 (from CALCE FAST library for SnAg solder)

Tensile fatigue strength exponent = -0.5 (from CALCE FAST)

Substrate Attributes (Copper)

Substrate thickness = 1250 μm = 1.25E-03 m (from lab measurement)

Elastic modulus = 110 GPa = 110E+09 (from Matweb)

Poisson's ratio = 0.343 (from Matweb for annealed copper)

CTE = 16.4 μm/m-°C = 16.4E-06 (from Matweb at 100°C)

Environment Attributes

Frequency of temperature cycles per day =

2000 cycles/day for Δ100°C (approximated from experimental data)

7500 cycles/day for Δ50°C (approximated from experimental data)

Temperature cycle =

Δ50°C and Δ100°C

Period definition = "hours"

Period length = 0

Appendix B: Power Dissipation Calculation

Power dissipation or loss consists of:

On-state power loss = $V_{CE(On)}$ * $I_{CE(On)}$ * Duty Cycle

Off-state power loss = $V_{CE(Off)}$ * $I_{CE(Off)}$* (1-Duty Cycle)

Switching power loss = Energy lost per switch * switching frequency

Energy lost per switch is provided in the data sheet as 329μJ, including the turn-on and turn-off losses.

The following parameters were determined from the experimental data at 175°C heat sink temperature or manufacturer's data sheet:

$V_{CE(On)}$, on-state voltage = 3.2 V (from experimental data at 175°C)

$V_{CE(Off)}$, off-state voltage = 10 V (from experimental data)

$I_{CE(On)}$, on-state current = 6 A (from experimental data at 175°C)

$I_{CE(Off)}$, off-state current = 0.3 A (from experimental data at 175°C)

DC, Switching duty cycle = 50% or 60% (set in the experiment)

Switching frequency = 1 kHz or 5 kHz (set in the experiment)

Switching loss = 329 μJ per switch (from data sheet at 175°C junction temperature)

An example calculation of power loss for 1 kHz switching frequency with 50% duty cycle is given in the following:

On-state Loss = $V_{CE(On)}$*$I_{CE(On)}$*DC = (3.4V)(6A)(50%) = 10.2 W

Off-state Loss = $V_{CE(Off)}$*$I_{CE(Off)}$*(1-DC) = (10V)(0.3A)(50%) = 1.5 W

Switching Loss = (329μJ)(1000Hz) = 0.329 W

Total Power Loss = 12.03 W

The resulting power losses for different combinations of switching frequencies and duty cycles are provided below:

	50% Duty Cycle	60% Duty Cycle
1 kHz Frequency	12.0 W	13.8 W
5 kHz Frequency	13.4 W	15.1 W

Appendix C: Classification Output Plots for Training Case 20/80

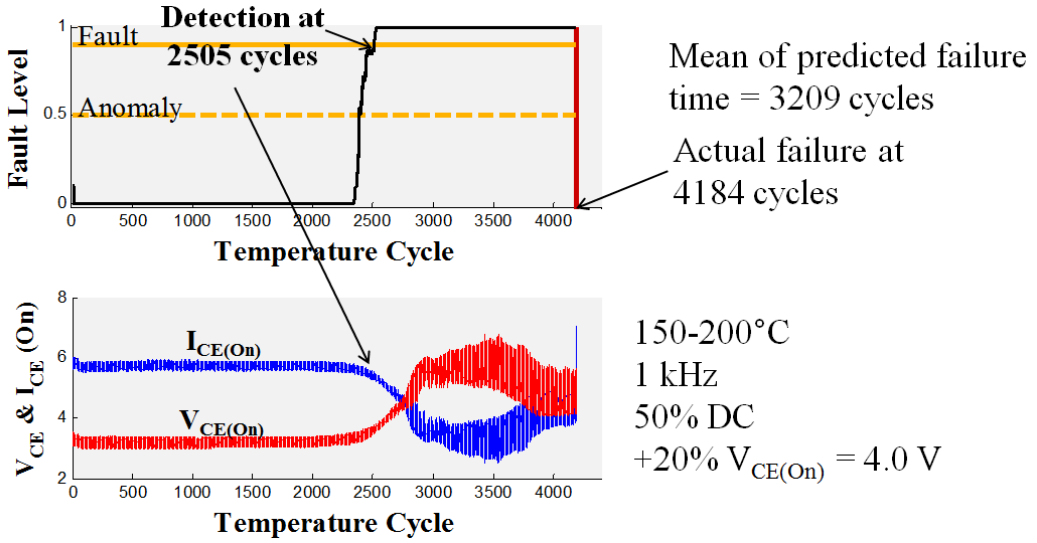

Figure 37 - IGBT#2

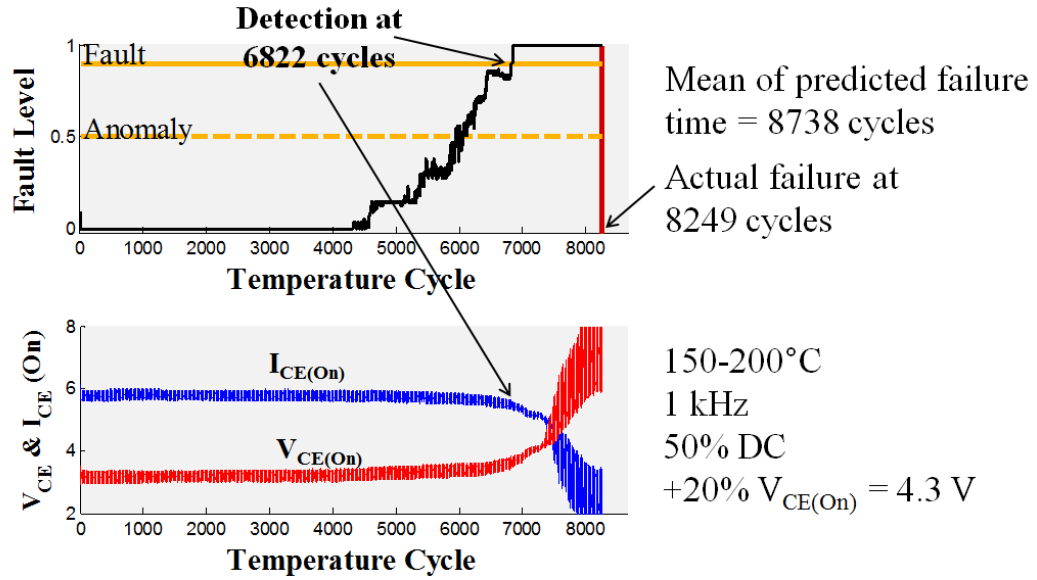

Figure 38 - IGBT#3

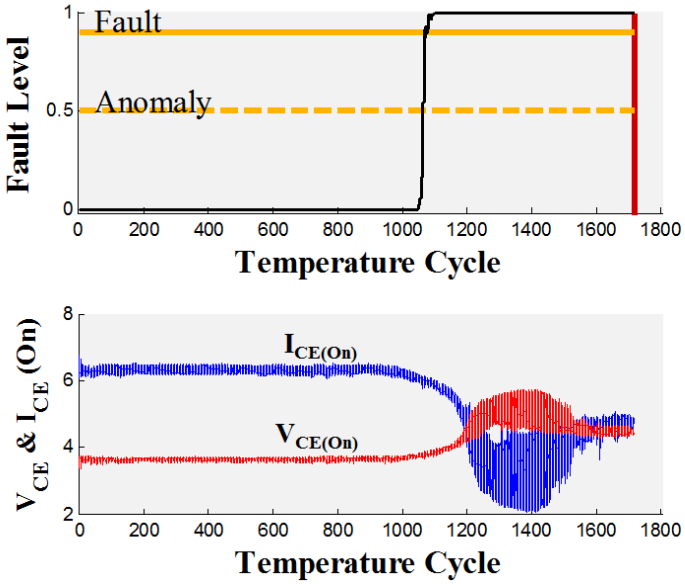

Detection at 1072 cycles.
Mean of predicted failure time = 1373 cycles.
Actual failure time = 1717 cycles.

150-200°C
1 kHz
60% DC
+20% $V_{CE(On)}$ = 4.4 V

Figure 39 - IGBT#4

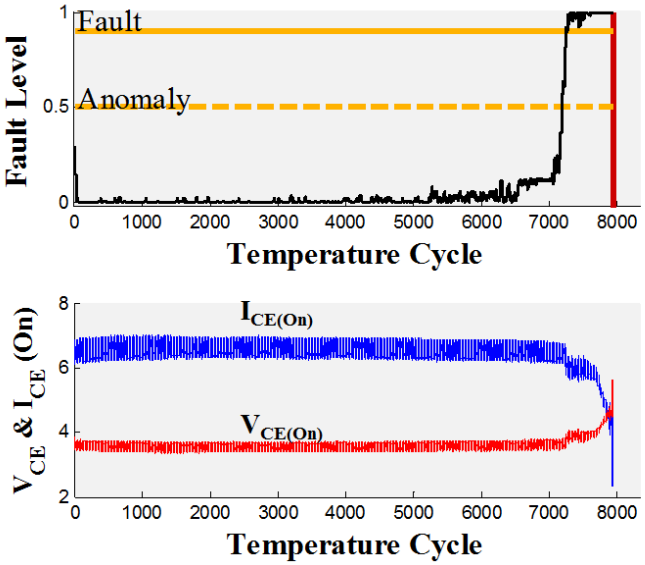

Detection at 7243 cycles.
Prediction mean failure time = 9278 cycles.
Actual failure time = 7927 cycles.

150-200°C
5 kHz
50% DC
+20% $V_{CE(On)}$ = 4.4 V

Figure 40 - IGBT# 6

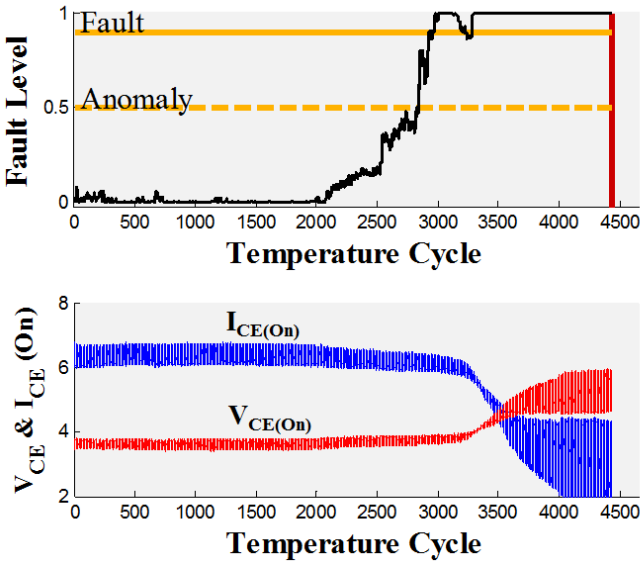

Detection at 2928 cycles.
Prediction mean failure time = 3751 cycles.
Actual failure time = 4428 cycles

150-200°C
5 kHz
60% DC
+20% $V_{CE(On)}$ = 4.4 V

Figure 41 - IGBT# 8

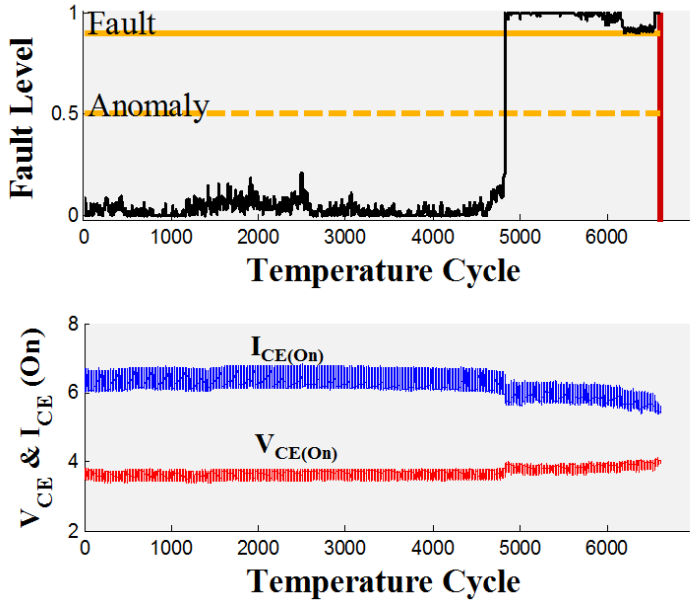

Detection at 4829 cycles.
Prediction mean failure time = 6186 cycles
Actual failure cycle = 6600 cycles.

150-200°C
5 kHz
60% DC
+20% $V_{CE(On)}$ = 4.4 V

Figure 42 - IGBT# 9

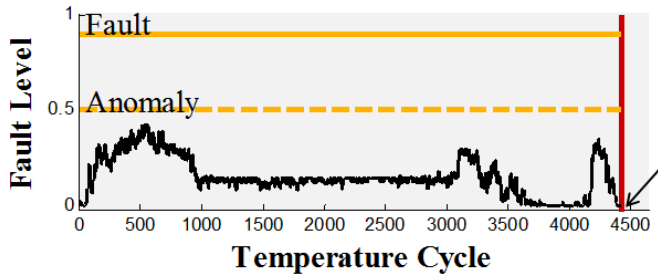

Failure at
4421cycles

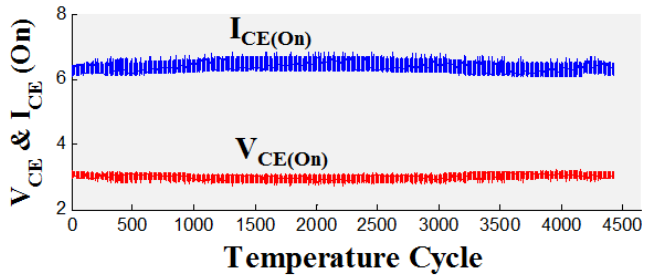

150-200°C
5 kHz
50% DC
+20% $V_{CE(On)}$ = 3.7 V

Figure 43 - IGBT# 10

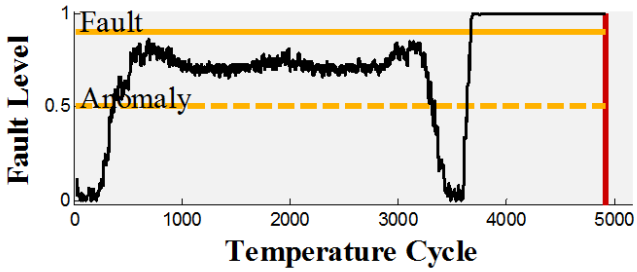

Detection at 3667 cycles.
Prediction mean failure time = 4697 cycles
Actual failure time = 4913 cycles

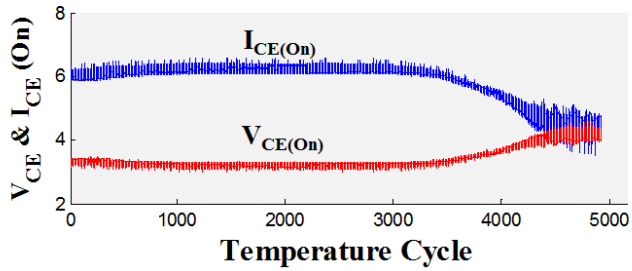

150-200°C
5 kHz
50% DC
+20% $V_{CE(On)}$ = 3.9 V

Figure 44 - IGBT# 11

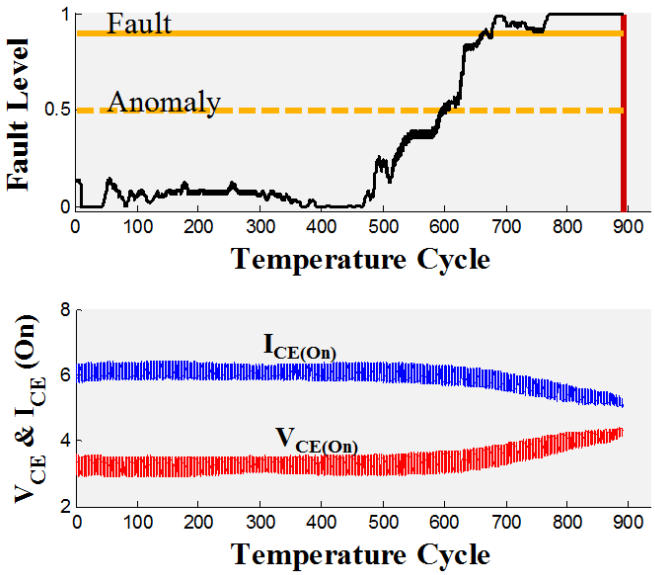

Detection at 662 cycles.
Prediction mean failure time = 848 cycles
Actual failure time = 891 cycles

125-225°C
1 kHz
50% DC
+20% $V_{CE(On)}$ = 3.9 V

Figure 45 - IGBT# 12

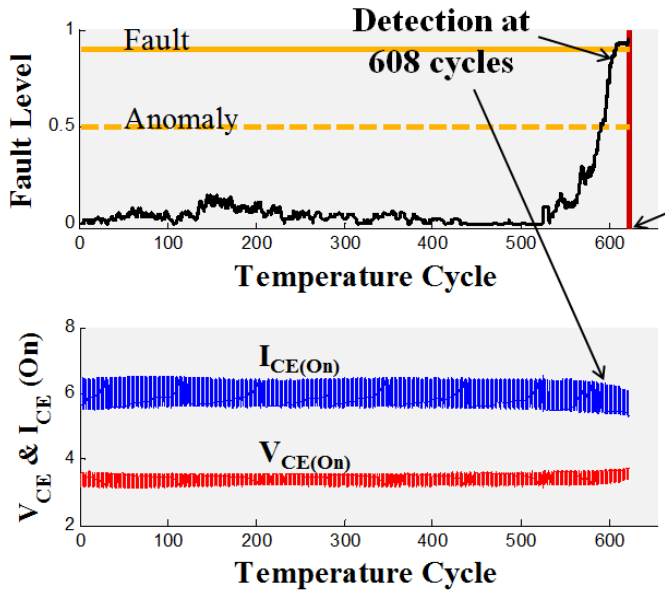

Mean of predicted failure time = 779
Actual failure at 623 cycles

125-225°C
1 kHz
50% DC
+20% $V_{CE(On)}$ = 4.2 V

Figure 46 - IGBT# 14

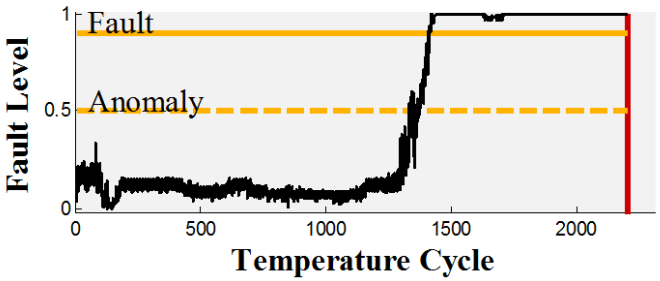

Detection at 1405 cycles.
Prediction mean failure time = 1800 cycles.
Actual failure time = 2200 cycles.

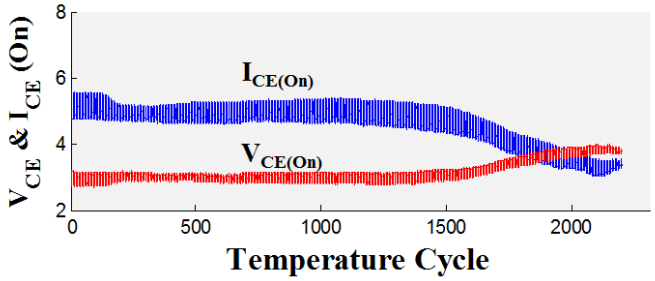

125-225°C
5 kHz
50% DC
+20% $V_{CE(On)}$ = 3.7 V

Figure 47 - IGBT# 16

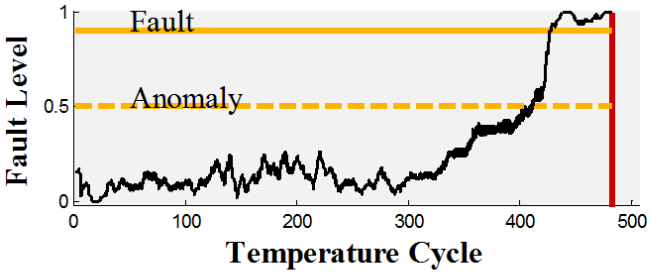

Detection at 427 cycles.
Prediction mean failure time = 547 cycles.
Actual failure time = 482 cycles.

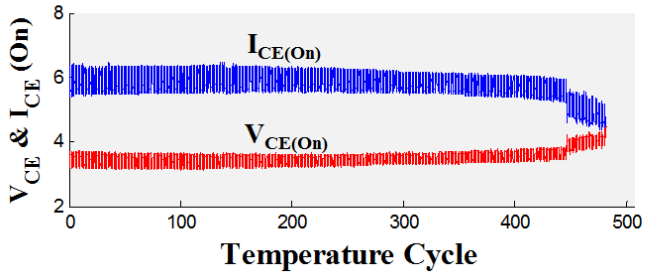

125-225°C
5 kHz
50% DC
+20% $V_{CE(On)}$ = 4.3 V

Figure 48 - IGBT# 17

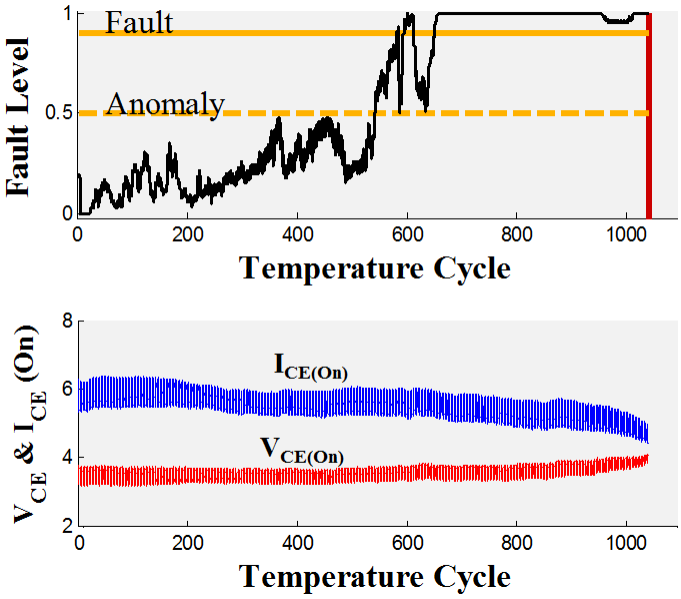

Detection at 583 cycles. Prediction mean failure time = 747 cycles. Actual failure cycle = 1040.

125-225°C
5 kHz
50% DC
+20% $V_{CE(On)}$ = 4.3 V

Figure 49 - IGBT# 18

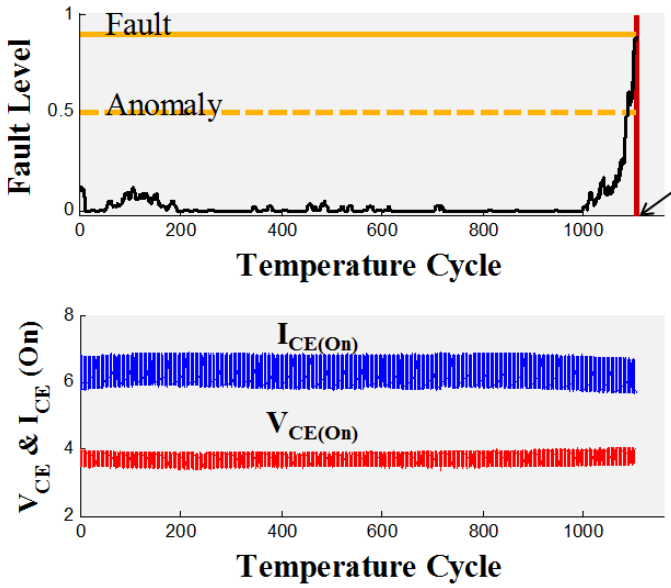

Failure at 1103 cycles

125-225°C
5 kHz switching
50% DC
+20% $V_{CE(On)}$ = 4.5 V

Figure 50 - IGBT# 20

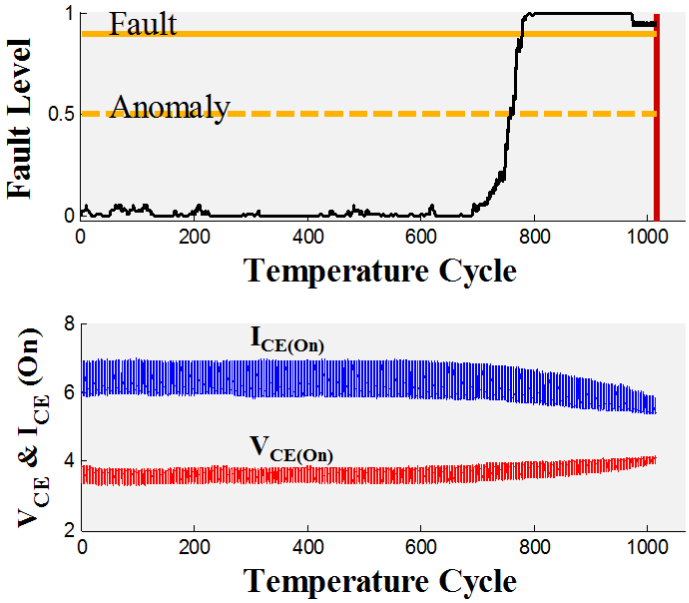

Detection at 778 cycles.
Prediction mean failure time = 997 cycles.
Actual failure time = 1014 cycles.

125-225°C
5 kHz
60% DC
+20% $V_{CE(On)}$ = 4.5 V

Figure 51 - IGBT# 22

Bibliography

[1] J. Baliga, "Enhancement and Depletion-Mode Vertical-Channel M.O.S Gated Thyristors," Electronics Letters, vol. 15, no. 20, pp. 645-647, 1979.

[2] A. Q. Huang, "Insulated Gate Bipolar Transistors," in The Power Electronics Handbook: Industrial Electronics Series, chapter 1.9, T.L. Skvarenina, Ed., CRC Press, 2002, pp. 1-77 - 1-81.

[3] V. Khanna, "IGBT: Theory and Design," IEEE Press/Wiley Interscience, Hoboken, NJ, 2003.

[4] S. Yang, A. Bryant, P. Mawby, D. Xiang, L. Ran, and P. Tavner, "An Industry-Based Survey of Reliability in Power Electronic Converters," IEEE Trans. on Industry Applications, vol. 47, no. 3, pp. 1441-1451, May/Jun. 2011.

[5] B. Lu and S. K. Sharma, "A Literature Review of IGBT Fault Diagnostic and Protection Methods for Power Inverters," IEEE Trans. on Industry Applications, vol. 45, no. 5, pp. 1770-1777, Sept./Oct. 2009.

[6] P. Tavner, "A Survey of Wind Turbine Condition Monitoring Experience in Europe," presentation at NREL 2011 Wind Turbine Condition Monitoring Workshop, Broomfield, CO, September 19-21, 2011.

[7] Reliawind, "Report on Wind Turbine Reliability Profiles," report deliverable D.1.3, issue 3, March 14, 2011.

[8] M. Held, P. Jacob, G. Nicoletti, P. Scacco, and M. H. Poech, "Fast Power Cycling Test for IGBT Modules in Traction Application," in Proc. 1997 International Conference on Power Electronics and Drive Systems, May 26-29, 1997.

[9] M. Ciappa, "Selected Failure Mechanisms of Modern Power Modules," Microelectronics Reliability, vol. 42, pp. 653-667, 2002.

[10] M. Bouarroudj, Z. Khatir, J.P. Ousten, F. Badel, L. Dupont, and S. Lefebvre, "Degradation behavior of 600V-200A IGBT modules under power cycling and high temperature environment conditions," Microelectronics Reliability, vol. 47, pp. 1719-1724, 2007.

[11] D. C. Katsis, and J. D. van Wyk, "Void-Induced Thermal Impedance in Power Semiconductor Modules: Some Transient Temperature Effects," IEEE Transactions on Industry Applications, vol. 39, no. 5, September/October 2003.

[12] V. Smet, F. Forest, J.J. Huselstein, F. Richardeau, Z. Khatir, S. Lefebvre, and M. Berkani, "Ageing and Failure Modes of IGBT Modules in High-Temperature Power Cycling," IEEE Transactions on Industrial Electronics, vol. 58, no. 10, October 2011.

[13] E. Suhir, “Stress in Adhesively Bonded Bi-Material Assemblies Used in Electronic Packaging,“ Proceedings of Material Research Society Symposium, vol. 72, pp. 133-138, 1986.

[14] E. Suhir, “Die Attachment Design and Its Influence on Thermal Stresses in the Die and the Attachment," Proceedings of 37th Electronic Components Conference, pp. 508-517, 1987.

[15] U.S. Department of Defense, “Military Handbook: Reliability Prediction of Electronic Equipment,” MIL-HDBK-217F, Notice 2, Washington D.C., Feb. 1995.

[16] C. Jais, B. Werner, and D. Das, ”Reliability predictions - continued reliance on a misleading approach,” Reliability and Maintainability Symposium, Orlando, Florida, 28-31 January, 2013.

[17] J. Gu and M. Pecht, “Health Assessment and Prognostics of Electronic Products: An Alternative to Traditional Reliability Prediction Methods,” Electronics Cooling, vol. 15, No. 2, pp. 10-16, 2009.

[18] S. Cheng, K. Tom, L. Thomas, and M. Pecht, “A Wireless Sensor System for Prognostics and Health Management,” IEEE Sensors Journal, vol. 10, no. 4, April 2010.

[19] Y. Xiong, Xu. Cheng, Z. Shen, C. Mi, H. Wu, and V. Garg, “Prognostic and Warning System for Power-Electronic Modules in Electric, Hybrid Electric, and Fuel-Cell Vehicles,” IEEE Trans. on Industrial Electronics, vol. 55, no. 6, pp. 2268-2276, June 2008.

[20] N. Patil, D. Das, and M. Pecht, “A Prognostic Approach for Non-Punch Through and Field Stop IGBTs,” Microelectronics Reliability, vol. 52, pp. 482-488, 2012.

[21] N. Patil, D. Das, and M. Pecht, “Mahalanobis Distance Approach for Insulated Gate Bipolar Transistors (IGBT) Diagnostics,” in Proc. International Conference on Concurrent Engineering, Cracow, Sept. 2010.

[22] N. Patil, S. Menon, D. Das, and M. Pecht, “Anomaly Detection of Non Punch Through Insulated Gate Bipolar Transistors (IGBT) by Robust Covariance Estimation Techniques,” in Proc. 2nd International Conference on Reliability, Safety & Hazard, pp. 68-72, Dec. 14-16, 2010.

[23] B. Saha, J. Celaya, P. Wysocki, and K. Goebel, "Towards Prognostics for Electronics Components," Proc. of the IEEE Aerospace Conference, Big Sky, MT, pp.1-7, 2009.

[24] J.R. Celaya, A. Saxena, S. Saha, and K.F. Goebel, “Prognostics of Power MOSFETs under Thermal Stress Accelerated Aging using Data-Driven and Model-Based Methodologies,” in Proc. Annual Conference of the Prognostics and Health Management Society, 2011.

[25] Y. Mitani and Y. Hamamoto, “A Local Mean-Based Nonparametric Classifier,” Pattern Recognition Letters, vol. 27, issue 10, pp. 1151-1159, July 15, 2006.

[26] S. Byers and A. E. Raftery, “Nearest-Neighbor Clutter Removal for Estimating Features in Spatial Point Processes,” Journal of the American Statistical Association, vol. 93, no. 442, pp. 577-584, June 1998.